

# Structure and evolution of Cenozoic arc magmatism on the Antarctic Peninsula: a high resolution aeromagnetic perspective

T.A. Jordan,<sup>1</sup> R.F. Neale,<sup>2,\*</sup> P.T. Leat,<sup>1,†</sup> A.P.M. Vaughan,<sup>1,‡</sup> M.J. Flowerdew,<sup>1,§</sup>  
T.R. Riley,<sup>1</sup> M.J. Whitehouse<sup>3</sup> and F. Ferraccioli<sup>1</sup>

<sup>1</sup>*British Antarctic Survey, High Cross, Madingley Road, Cambridge, CB3 0ET, United Kingdom. E-mail: tomj@bas.ac.uk*

<sup>2</sup>*School of Earth and Environment, University of Leeds, Leeds LS2 9JT, United Kingdom*

<sup>3</sup>*Swedish Museum of Natural History, Box 50007, Stockholm 104 05, Sweden*

Accepted 2014 June 17. Received 2014 June 12; in original form 2014 February 11

## SUMMARY

The Antarctic Peninsula (AP) consists of a long lived and uniquely well preserved magmatic arc system. The broad tectonic structure of the AP arc is well understood. However, magmatic processes occurring along the arc are only constrained by regional geophysical and relatively sparse geological data. Key questions remain about the timing, volume, and structural controls on magma emplacement. We present new high resolution aeromagnetic data across Adelaide Island, on the western margin of the AP revealing the complex structure of the AP arc/forearc boundary. Using digital enhancement, 2-D modelling and 3-D inversion we constrain the form of the magnetic sources at the arc/forearc boundary. Our interpretation of these magnetic data, guided by geological evidence and new zircon U-Pb dating, suggests significant Palaeogene to Neogene magmatism formed ~25 per cent of the upper crust in this region (~7500 km<sup>3</sup>). Significant structural control on Neogene magma emplacement along the arc/forearc boundary is also revealed. We hypothesize that this Neogene magmatism reflects mantle return flow through a slab window generated by Late Palaeogene cessation of subduction south of Adelaide Island. This mantle process may have affected the final stages of arc magmatism along the AP margin.

**Key words:** Magnetic anomalies; modelling and interpretation; Mantle processes; Volcanic arc processes; Continental margins: convergent; Crustal structure; Antarctica.

## 1 INTRODUCTION

The magmatic arc along the Antarctic Peninsula (AP) once formed part of the tectonically active circum Pacific ‘ring of fire’. Cessation of subduction due to Cenozoic ridge-trench collision along the AP has preserved an intact arc/forearc system (Larter & Barker 1991). The AP therefore provides a snapshot of arc processes during the final stages of subduction. The regional magmatic and tectonic evolution of the AP arc is inferred from reconnaissance aeromagnetic data, and geological observations of relatively sparse outcrops (Leat *et al.* 1995; Ferraccioli *et al.* 2006; Vaughan *et al.* 2012a). However,

critical questions remain about the volume of arc magmatism, migration of the arc through time, and the extent of structural control on the evolution of the arc magmatic system.

One key area of the AP where many questions remain is along the arc/forearc boundary, where the latest phases of arc magmatism are thought to have occurred. Here we use recently acquired high resolution aeromagnetic data over Adelaide Island, on the western margin of the AP (Figs 1 and 2), to investigate the processes occurring along the arc/forearc boundary. High resolution aeromagnetic data has elsewhere been used to reveal tectonic structures in forearc regions (Ponce *et al.* 2003; Saltus *et al.* 2005), the geometry of arc magmatic intrusions (De Ritis *et al.* 2010), and tectonic and magmatic patterns in rift systems formed along the reactivated margins of older magmatic arc terranes (Ferraccioli *et al.* 2005). We apply digital enhancement, 2-D modelling and 3-D inversion to the new magnetic data in order to reveal the structure of the AP arc/forearc boundary. Additionally, new U-Pb geochronological evidence for an extended period of magmatism on the western margin of the AP is presented. Our results are interpreted to show the volume and varied structural control of magmatism at the arc/forearc boundary.

\*Now at: ION GX Technology, 578-586 Murray Street, West Perth, WA 6005, Australia.

†Now at: Department of Geology, University of Leicester, University Road, Leicester LE1 7RH, United Kingdom.

‡Now at: Midland Valley, 144 W George St, Glasgow, Lanarkshire G2 2HG, United Kingdom.

§Now at: CASP, University of Cambridge, West Building, 181A Huntingdon Road, Cambridge CB3 0DH, United Kingdom.

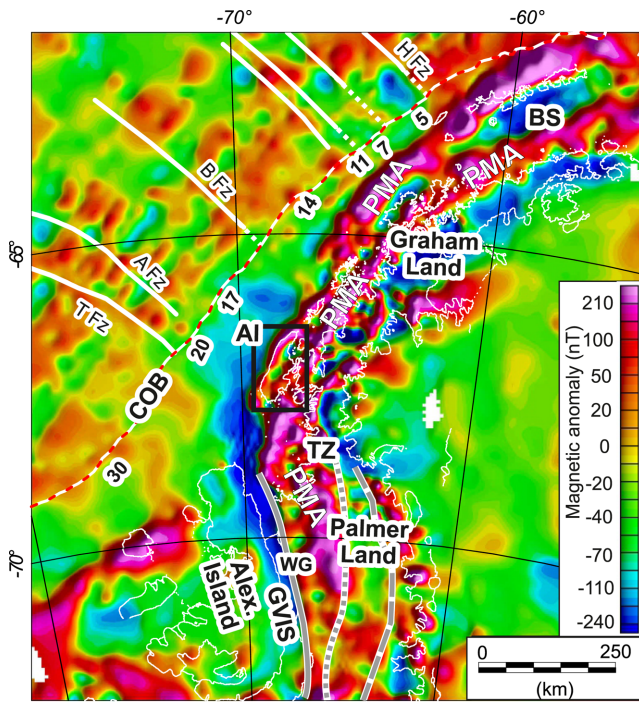


**Figure 1.** Regional aeromagnetic anomaly map over the Antarctic Peninsula (Golynsky *et al.* 2001), centred on Adelaide Island (AI). Displayed data were predominantly collected between 1.25 and 2.5 km altitude (Johnson 1999), and were interpolated onto a 5 km grid (Golynsky *et al.* 2001). Black box locates Fig. 2. Thin white line marks the coast. Thick white lines mark fracture zones (Larter & Barker 1991) (TFz, Tula Fracture Zone; AFz, Adelaide Fracture Zone; BFz, Bisco Fracture Zone; HFz, Hero Fracture Zone). Red and white dashed line marks the continent ocean boundary (COB), and numbers mark inferred age (Ma) of ridge/trench collision and cessation of subduction (Larter & Barker 1991). Grey lines mark the sutures between inferred Palmer Land terranes (Ferraccioli *et al.* 2006; Vaughan *et al.* 2012a). Note the Pacific Margin Anomaly (PMA), the major positive magnetic anomaly running along the peninsula, which splits in two either side of Bransfield Strait (BS). TZ, Transition Zone; WG, Wiley Glacier; GVIS, George VI Sound; Alex. Island, Alexander Island.

Our findings are discussed in terms of the structural and magmatic evolution during the final, Cenozoic stages of subduction, providing new insights on the driving mechanisms for AP arc magmatism.

## 2 GEOLOGICAL AND GEOPHYSICAL SETTING

### 2.1 Regional tectonic setting

The AP is dominated by a former magmatic arc, which developed as a result of subduction processes along the margin of Gondwana, with the earliest elements in place by Early Jurassic times (Leat *et al.* 1995; Vaughan *et al.* 2012b). Geological and geophysical data suggest that subduction along the AP was punctuated by the mid-Cretaceous accretion of allochthonous terranes to form a composite magmatic arc (Fig. 1; Vaughan & Storey 2000; Ferraccioli *et al.* 2006; Vaughan *et al.* 2012a; Yegorova & Bakhmutov 2013). Late Cretaceous to Neogene progressive collision of spreading ridge segments, separated by fracture zones, at the continent ocean boundary shut down the subduction system from south to north (Fig. 1). Subduction now only continues at the northern tip of the AP, north of Bransfield Strait (Larter & Barker 1991).

Field studies show that magmatism played a key role throughout the evolution of the AP (Leat *et al.* 1995). Voluminous granitic and silicic volcanic rocks were emplaced in Mid-Jurassic times (Riley & Leat 1999). During the Early Cretaceous a significant period of tonalite-granodiorite magmatism occurred, with plutons emplaced within extensional shear zones, predominantly exposed along the western margin of the AP adjacent to George VI Sound (Vaughan *et al.* 1997, 1998). Continued magmatism, in the early Cenozoic, is associated with transtension (Leat *et al.* 2002). A general westward progression in magmatism is suggested (Parada *et al.* 1992), and Cenozoic magmatism appears to dominate the islands along the western edge of the AP (Riley *et al.* 2012). As mentioned above, arc magmatism stopped following the progressive cessation of subduction between ~50 Ma and the present (McCarron & Larter 1998). Post-arc magmatism is represented by emplacement of a suite of alkali basalts (Hole *et al.* 1991), linked to the formation of slab windows behind the subducted ridge crest and associated asthenospheric upwelling (Hole *et al.* 1991).

Geophysical evidence for extensive magmatism along the AP comes from reconnaissance aeromagnetic studies, flown at ~3 km line spacing and 1250–2500 m altitude, (Fig. 1), which reveal the ca. 1500-km-long positive magnetic Pacific Margin Anomaly (PMA) associated with the arc batholith (Storey & Garrett 1985). As magmatism along the AP was long lived (Leat *et al.* 1995) the precise timing of emplacement of the batholith that causes the PMA is controversial. Originally, the PMA was modelled as a series of ~20-km-thick mafic arc batholiths emplaced diachronously within an extensional overriding plate (Storey & Garrett 1985; Garrett 1990; Leat *et al.* 1995). Other studies suggested a predominantly Cretaceous age for the PMA, at least in the southern AP, where the PMA correlates with Early Cretaceous syn-extensional plutons exposed around Wiley Glacier in Palmer Land (Vaughan *et al.* 1998). This Cretaceous model for the PMA implies rapid and widespread generation and emplacement of significant volumes of magma. Extensive magnetic susceptibility measurements of AP igneous rocks yield highly variable values, although gabbros tend to yield the highest susceptibility values (Wendt *et al.* 2013). This suggests that neither a specific rock type nor its age can be directly inferred from the presence of the PMA.

The internal structure of the PMA is also controversial. To the south of Adelaide Island, the PMA is offset between Palmer Land and Graham Land by a ‘transition zone’ (Fig. 1), linked to fracture zone intersection with the margin, transtension along the AP and extension in George VI Sound (Garrett 1990; Johnson & Swain 1995). However, conflicting sinistral and dextral Cenozoic strike-slip motions have both been proposed for this region (Johnson & Swain 1995; Johnson 1997; Noltimier 1998). To the north of Adelaide Island the PMA comprises two parallel anomalies. Johnson (1999) proposed that an original single batholith was split along its axis to form the parallel magnetic anomalies, although he also discussed an alternative hypothesis that the parallel anomalies are original features representing two separate arcs. A third model in which the western branch of the PMA is a Cretaceous allochthonous terrane has also been suggested (Yegorova *et al.* 2011; Yegorova & Bakhmutov 2013).

Adelaide Island (Figs 1 and 2) provides an ideal area to investigate the later stage evolution of the AP arc, as the geology of this region is relatively well studied (Riley *et al.* 2012), and it lies on the western margin of the AP at the arc/forearc boundary. Additionally regional aeromagnetic studies suggest Adelaide Island lies between the more tectonically complex transition zone and the main split in the PMA.

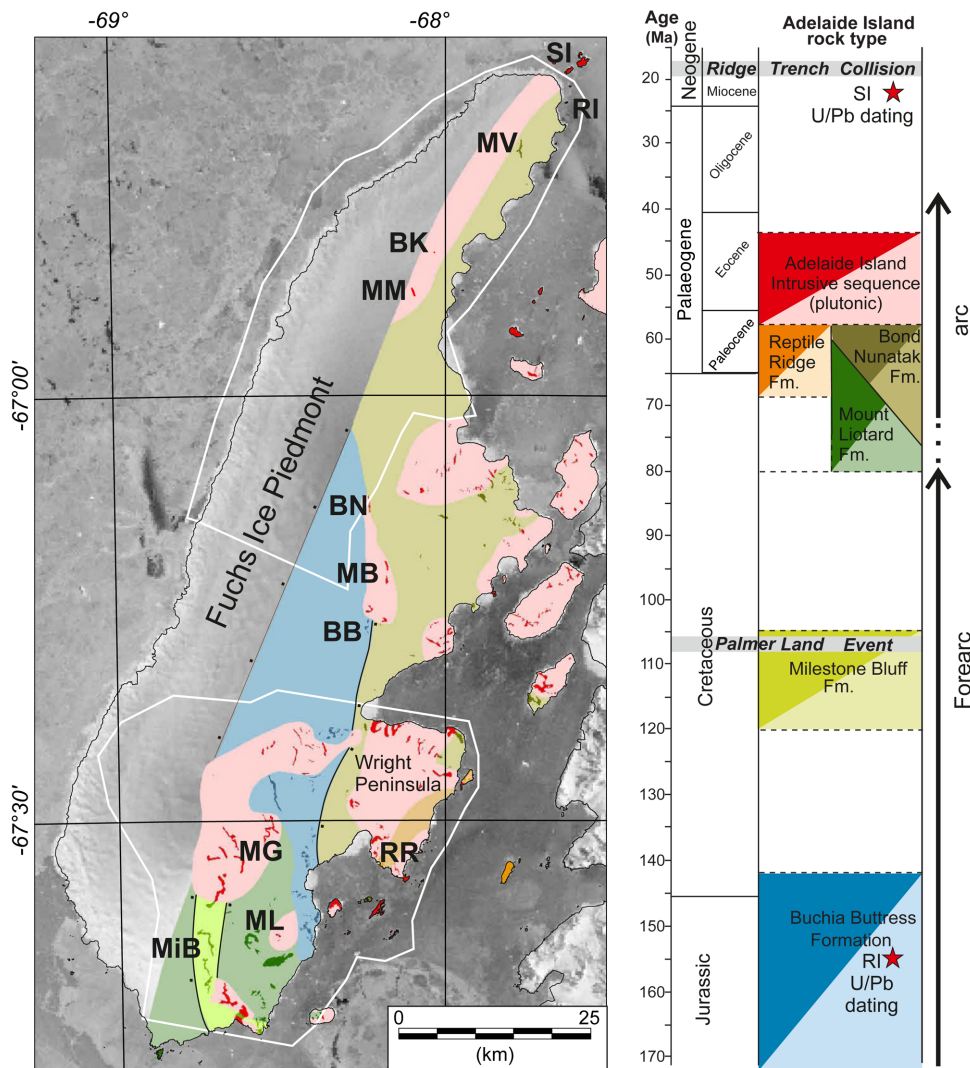


**Figure 2.** Geological map and stratigraphic column of Adelaide Island (Riley *et al.* 2012). Background image shows RAMP satellite mosaic (Jezek & RAMP-Product-Team 2002). White outlines mark new aeromagnetic surveys. Solid colours mark rock outcrop. Pale colours show inferred geology. Red stars on stratigraphic column mark ages presented in this paper for rocks from the Sillard Islands (SI) and Rigsby Island (RI). Other place names as follows from north to south: MV, Mt Vélain; BK, Blümcke Knoll; MM, Mt Machatschek; BN, Bond Nunatak; MB, Mt Bouvier; BB, Buchia Buttress; MG, Mt Gaudry; RR, Reptile Ridge; ML, Mt Liotard; MiB, Milestone Bluff. Note gaps in stratigraphic column reflect gaps in rock exposure, rather than a mapped hiatus in deposition.

## 2.2 Geology of Adelaide Island

Adelaide Island is situated off the west coast of the AP, to the north of Alexander Island (Fig. 1). The island is divided into two distinct topographic areas: the Fuchs Ice Piedmont to the west, and a mountainous area on the eastern/central part of the island, including the massifs of Mts Bouvier, Gaudry and Liotard (Figs 2 and 3). Almost all rock exposure is on the eastern side of the island, and is generally restricted to isolated, often hard to access outcrops. The geology was first described in the 1970s (Dewar 1970), and revisited in the 1990s, with a probable Late Jurassic age proposed for the stratified rocks (Griffiths & Oglethorpe 1998). A revised stratigraphy of Adelaide Island was proposed (Riley *et al.* 2012), using more recent geological mapping (Fig. 2) and newly acquired geochronology, combined with the previous field studies (Dewar 1970; Griffiths & Oglethorpe 1998), and spectral mapping (Haselwimmer *et al.* 2010). Together the succession of sedimentary, volcanoclastic and volcanic rocks on Adelaide Island reflects the transition in setting from a forearc

in Jurassic to mid Cretaceous times, to an arc in the Late Cretaceous and Early Cenozoic. Correlations with rocks on Alexander Island ~250 km to the south suggest that this forearc/arc sequence is laterally extensive along the margin of the AP (Riley *et al.* 2012).

### 2.2.1 Adelaide Island sedimentary and volcanic rocks

Adelaide Island preserves a 2–3-km-thick succession of sedimentary, volcanic and associated volcanoclastic rocks, interpreted to be Jurassic to Cretaceous in age (Fig. 2). The oldest sequences include the Buchia Buttress, and Milestone Bluff formations, composed of immature volcanoclastic rocks with interbedded cobble/boulder conglomerates and sandy turbiditic beds. U-Pb zircon geochronology of a crystal tuff in the Buchia Buttress Formation gives a date of  $149.5 \pm 1.6$  Ma (Riley *et al.* 2012), in agreement with the interpreted Late Jurassic molluscan fauna preserved at Buchia Buttress (Thompson 1972). The younger Milestone Bluff Formation is dated

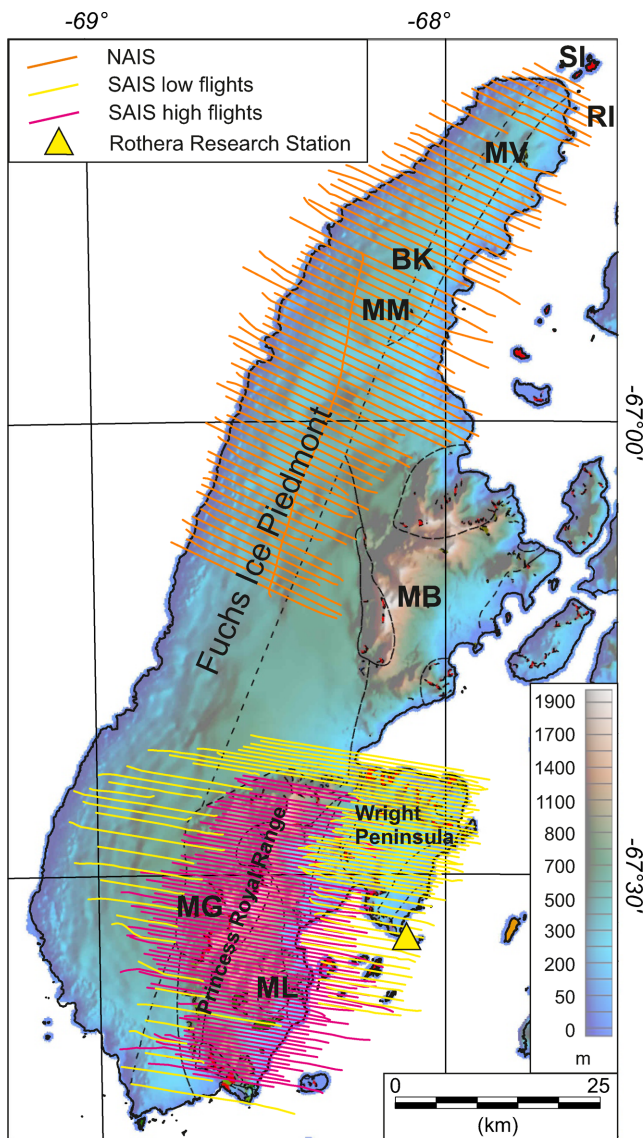


**Figure 3.** Survey flight lines across Adelaide Island. Background image shows Digital Elevation Model (Cook *et al.* 2012). NAIS, Northern Adelaide Island Survey; SAIS, Southern Adelaide Island Survey. Note for clarity tie lines are not shown for the SAIS survey. Dashed lines and coloured regions show inferred geological boundaries and rock outcrop from Fig. 2.

from rare ignimbrites to  $113.9 \pm 1.2$  Ma (Riley *et al.* 2012). Conglomerate clast orientations in the Milestone Bluff Formation indicate a general sediment source from the east or southeast (Griffiths & Oglethorpe 1998; Riley *et al.* 2012). Plutonic clasts have been dated at  $\sim 140$  Ma (Griffiths & Oglethorpe 1998) consistent with derivation from the Cretaceous batholiths to the southeast in NW Palmer Land (Fig. 1, e.g. Vaughan *et al.* 1997).

The younger sequences of sedimentary and volcanic rocks on Adelaide Island include the Bond Nunatak, Mt Liotard and Reptile Ridge formations. The former two sequences were deposited coevally, and consist of basaltic andesite and andesite lava flows, with some interleaved sandstones and conglomerates. These have an estimated age of  $\sim 75$  Ma, based on correlated units (Riley *et al.* 2012). The Reptile Ridge Formation is dated to  $67.56 \pm 0.72$  Ma (Riley *et al.* 2012), and consists of poorly bedded and hydrothermally altered rhyolite-rhyodacite crystal tuffs, lithic tuffs, ignimbrites and rare lava flows.

### 2.2.2 Adelaide Island intrusive suite

A large part of the exposed geology on Adelaide Island consists of plutonic rocks of the Adelaide Island Intrusive Suite (AIIS; Fig. 2). The area around Mount Gaudry is dominated by tonalites, whereas Wright Peninsula predominantly consists of granodioritic and gabbroic rocks, suggesting separate phases of intrusion. Many of the plutons are heterogeneous and are characterized by concentrations of well-rounded, typically more mafic, xenoliths. At several localities the plutonic rocks are observed to have intruded the sedimentary and volcanic successions (Dewar 1970). The final phase of magmatism, noted in the southern part of Adelaide Island, is a series of intrusive dykes cross cutting many of the plutons, and the surrounding volcanic sequences (Riley *et al.* 2012). Although not dated, these dykes clearly post-date the main phase of plutonism on southern Adelaide Island, and exhibit a distinct north–northeast trend (Riley *et al.* 2012).

To the north of Adelaide Island, intrusive rocks are exposed on a number of offshore islands, and in small outcrops in the Fuchs Ice Piedmont. Unlike the intrusive rocks in the south of Adelaide Island, the intrusive quartz diorites on the Sillard Islands (Fig. 2) show vertical banding with a dominantly north–south trend, originally linked to magma flow (Goldring 1959). Similar subvertical magmatic ‘flow bands’ are also described in diorites at Blümcke Knoll (Fig. 2; Dewar 1962). Syn-emplacment deformation as a possible cause for similar structures in Palmer Land has also been proposed (Vaughan *et al.* 1997). On Rigsby Island, deformed tonalites are present, which show horizontally orientated slickensides indicating strike slip motion (Goldring 1959, 1962).

Griffiths & Oglethorpe (1998) dated three granodiorite samples from the Wright Peninsula area (Fig. 2) using fission track dating (apatite and zircon) yielding ages of  $44.2 \pm 3.8$ ,  $52.0 \pm 2.9$  and  $52.4 \pm 3.5$  Ma. Riley *et al.* (2012) dated a tonalite from near Mt Bouvier (Fig. 2) to  $47.3 \pm 0.4$  Ma using U–Pb (zircon). These Eocene ages for plutonism on Adelaide Island significantly post-date the main phases of sedimentation and volcanism. New U–Pb zircon dating of intrusive rock samples from the Sillard Islands and Rigsby Island (see supplementary material for detail), give well defined, but contrasting ages of  $22.9 \pm 0.2$  and  $156.4 \pm 0.9$  Ma, respectively. The youngest date precedes the cessation of subduction at this latitude by only  $\sim 6$  Ma (Larter & Barker 1991), indicating these rocks represent the final phase of arc magmatism in this region. The older age would be consistent with the last part of a Mid-Jurassic pulse of more acidic arc magmatism noted along the AP, thought to be associated with the extensional breakup of Gondwana (Leat *et al.* 1995; Riley & Leat 1999). The wide range of our new ages (Fig. 2) highlights the complex and long lived nature of magmatism on Adelaide Island.

## 3 METHODS

### 3.1 Aeromagnetic data collection and processing

Two aeromagnetic surveys were carried out during the 2010–2011 field season in order to investigate the subsurface geology of the arc and forearc region on Adelaide Island (Fig. 3). Aeromagnetic data were collected using two wingtip mounted Scintrex caesium magnetometers fitted to the British Antarctic Survey geophysically equipped Twin Otter aircraft (Ferraccioli *et al.* 2007).

The first survey was a dedicated high resolution aeromagnetic survey (HRAM) over the Princess Royal Range and the Wright Peninsula (Fig. 3), hereafter the Southern Adelaide Island Survey.

The Southern Adelaide Island Survey was flown at two draped levels due to the extreme topographic variation over the survey area (>1000 m vertical over <1.5 km horizontal), which could not be draped by our survey aircraft. The lower level was flown draped at ~250 m above the ice surface, and covered parts of the Fuchs Ice Piedmont and Wright Peninsula. The upper survey level, over the Princess Royal Range, draped the island's peak topography (2565 m). The upper and lower survey levels overlapped by at least 5 km to facilitate merging of the data sets. The survey was flown with 500 m line spacing, with tie lines every 2 km. Data were corrected for motion of the aircraft (compensation correction), the International Geomagnetic Reference Field (IGRF), and diurnal variations in the magnetic field measured at a temporary magnetic base station at Rothera Research Station (Fig. 3). The average range to the base station was ~21 km, and the maximum distance was ~44 km. The magnetic data were upward or downward continued from the flight elevation to a level ~250 m above the surface. The continuation method used allowed suppression of short wavelength instability associated with downward continuation (Pilkington & Thurston 2001). Statistical levelling was then applied first to the tie line and then the line data, giving a crossover error of ~9 and ~19 nT for the high and low cap, respectively. The data were then gridded with a 100 m mesh and microlevelling was applied to remove residual corrugations in the data (Ferraccioli *et al.* 1998). The data from the two drape levels was adjusted separately, and then merged using the Geosoft™ gridknit function, which smoothly joins the grids while preserving the wavelength character of the data. After merging the aeromagnetic data were reduced to the pole (RTP) to minimize the asymmetry in anomalies create by the local inclination of the Earth's magnetic field (Fig. 4).

The second survey covered the Fuchs Ice Piedmont and the northern part of Adelaide Island (Fig. 3), hereafter the Northern Adelaide Island Survey. This survey was flown principally for airborne radar measurement of ice thickness, with coincident opportunistic collection of aeromagnetic data. These survey flights were draped at ~250 m above the ice surface, giving an approximate distance to source of 750 m, assuming an average ice thickness of ~500 m from preliminary analysis of radio echo sounding data. The survey had 1 km line spacing, and aeromagnetic data were processed as for the Southern Adelaide Island Survey. The average range to the base station was ~74 km, and the maximum distance was ~107 km. Due to the opportunistic nature of the aeromagnetic data acquisition, no magnetic compensation calibration was carried out for the northern survey. Additionally, only one partial tie-line was collected (Fig. 3). Aeromagnetic data were therefore interpolated onto a 200 m mesh grid, and further improvement of the data relied on microlevelling techniques (Ferraccioli *et al.* 1998). The final aeromagnetic anomaly map shows no obvious line related artefacts (Fig. 4).

### 3.2 Digital enhancement of aeromagnetic data

To enable a better understanding of the geological structures across Adelaide Island, a range of digital enhancement techniques were applied to the primary RTP aeromagnetic signal. The aim of these techniques was to enhance the visibility of structural trends, and to resolve the location of source body margins, through mathematical transformation of the data.

An automatic gain correction (AGC) filter was applied to enhance separation of local signals from the regional background field. This technique works by normalizing the anomaly amplitude within a moving window (Rajagopalan & Milligan 1994). We found a

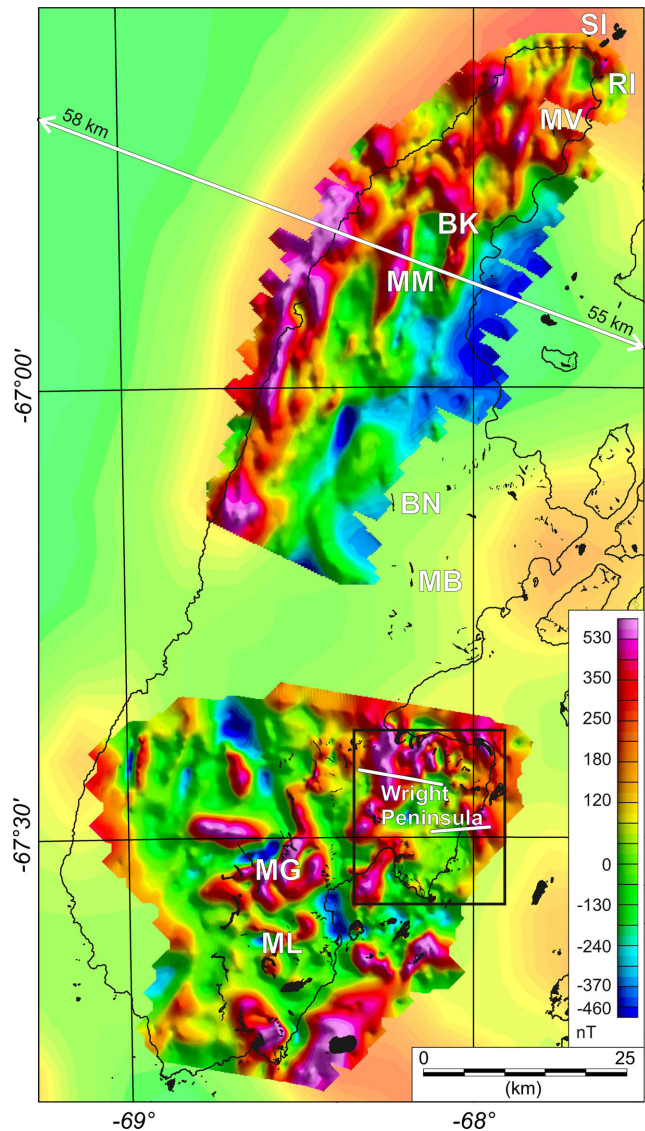


**Figure 4.** Aeromagnetic data over Adelaide Island. Background image shows semi-transparent regional magnetic data from ADMAP compilation (Golynsky *et al.* 2001). Black lines show coast and rock outcrop. Note separate Northern Adelaide Island Survey, revealing north–northeast trending linear structures, and the Southern Adelaide Island Survey with no dominant trend. White lines show modelled profiles. Black numbers indicate extension of the regional Northern Adelaide Island Survey profile beyond this figure (Fig. 8a). Black box locates Fig. 5.

window size of 1.5 km and a maximum gain correction of 10 gave good enhancement of the shallow structures across Adelaide Island, while retaining resolution of areas of regionally high or low magnetic intensity.

The normalized maximum horizontal gradient amplitude of the tilt derivative (TDX) was calculated to enhance the location of source body margins (Cooper & Cowan 2006). This enhancement is calculated as the inverse tangent of the ratio of the maximum horizontal and vertical gradients of the magnetic field. By defining a threshold value of 1.16 rad the theoretical edges of the source bodies were plotted across the survey area. Qualitatively broader areas of high TDX relate to deeper sources, while narrow bands of high TDX suggest shallow source bodies.

To enhance the deeper sources across Adelaide Island pseudo gravity values were calculated (Cordell & Grauch 1985; Blakely & Simpson 1986). This transformation integrates the rotated to pole magnetic field and calculates the equivalent gravity anomaly assuming all magnetic sources have the same specific density contrast (Blakely & Simpson 1986). We chose a standard specific density contrast of  $1000 \text{ kg m}^{-3}$ , and an assumed magnetization of 0.5 gauss.

The locations of anomaly peaks were extracted from the AGC filtered grid to help delineate lineations across our survey area. We followed the technique of previous authors to extract the locations of peaks and ridges where grid values in at least two directions were lower (Blakely & Simpson 1986). To calculate lineation direction, we developed a brute-force search technique to sort the peak locations from the AGC filtered data into separate lineation segments, up to 25 points long, with a maximum gap between points along the lineation of 600 m. The strike and length of each lineation segment was calculated by fitting a linear trend through the segment points. This allowed rose diagrams of lineation orientation to be automatically produced.

The final digital enhancement we applied was to calculate the apparent susceptibility (Hinze *et al.* 2013). This is the susceptibility of a collection of idealized vertical prisms of infinite depth, which would give rise to the observed magnetic field. Results of this digital enhancement were compared to existing susceptibility measurements across the AP (Wendt *et al.* 2013), and new susceptibility measurements we made on rock samples from Rigsby Island and the Sillard Islands, just north of Adelaide Island (Fig. 4).

## 4 RESULTS

### 4.1 New aeromagnetic anomaly map

Our new aeromagnetic anomaly map of Adelaide Island (Fig. 4) broadly agrees with previous regional studies (Johnson 1999; Golynsky *et al.* 2001) although significantly shorter wavelength detail is now resolved. The Southern Adelaide Island Survey shows significant high amplitude ( $>1000 \text{ nT}$ ) short wavelength (1–2 km) anomalies over Wright Peninsula and Mt Gaudry. These anomalies do not show a dominant regional trend, although linear anomaly margins suggest a degree of structural control of the source bodies.

The Northern Adelaide Island Survey shows a series of linear 10–20-km-long north–northeast trending anomalies with amplitudes of 300–800 nT, and wavelengths of 2–3 km (Fig. 4). One of these anomalies correlates with rock outcrops at Mt Machatschek and Blümcke Knoll. However, rock outcrops at Mt Vélain and on the adjacent small islands were not overflowed. A strong west to east gradient in the magnetic field is apparent across the Northern Adelaide Island Survey. This is consistent with the regional magnetic data, which shows that the Northern Adelaide Island Survey samples the eastern flank of a  $\sim 30 \text{ km}$  wavelength linear positive magnetic anomaly, with a north–northeast to northeast trend, thought to be part of the western PMA (Johnson 1999). In the southeast corner of the Northern Adelaide Island Survey, close to Bond Nunatak, an arcuate anomaly with amplitude of  $\sim 200 \text{ nT}$  and a wavelength of 3–4 km is observed (Fig. 4).

### 4.2 Digital enhancement across Wright Peninsula

The geology of Wright Peninsula is relatively well constrained (Fig. 5a), due to more abundant rock out-crop and proximity to

Rothera Research Station (Riley *et al.* 2012). The peninsula is dominated by igneous intrusive rocks of the AIIIS, which have a range of compositions, but are dominated by gabbros and granodiorites. AGC enhancement of the magnetic data reveals a northeasterly trend on the western side of the peninsula, and a series of approximately linear north–northwest trending structures (Fig. 5b). Many of these short wavelength anomalies correlate well with outcrops of the AIIIS, suggesting these igneous rocks are likely the main source for the observed positive magnetic anomalies. A pseudo gravity filter across Wright Peninsula (Fig. 5c) shows that positive anomalies, and associated deeper magnetic sources, are focused around the margins of the peninsula. Many of the high frequency anomalies revealed by the AGC filter (Fig. 5b) are not visible, indicating the source bodies are shallow structures. The TDX map of Wright Peninsula (Fig. 5d) provides an alternative view of the margins of the geological source bodies, compared to the existing geological map. Most of the magnetic sources appear to lie around the margins of Wright Peninsula, while the central and southern region shows few clear magnetic sources. Very narrow bands with high TDX values across the northern Wright Peninsula suggest very shallow magnetic sources (Fig. 5d).

### 4.3 Structural variation across Adelaide Island

The trends and boundaries of the magnetic sources across Adelaide Island are revealed by a series of further digital enhancements (Fig. 6). The pseudo gravity filter (Fig. 6a) reveals the deeper magnetic sources. This enhancement confirms the overall pattern noted in the RTP field (Fig. 4). However, a regional north easterly trend, in addition to the more localized north–northeast trends, becomes apparent across the Northern Adelaide Island Survey area. The fact that the north–northeast trends are not totally removed by this filter suggests that the source bodies are relatively deep seated. The more varied and complex trends noted in the Southern Adelaide Island Survey RTP field are also confirmed, with both northwesterly and northeasterly trending anomalies visible over Mt Gaudry and Wright Peninsula respectively.

The TDX enhancement of the anomaly margins (Fig. 6b) gives an estimation of the shape and extent of potential near surface source bodies. This definition of anomaly margins shows that the linear anomalies around Mt Machatschek and Blümcke Knoll continue further south along strike than would be apparent in the RTP data. However, it is also apparent that the linear north–northeast trending anomalies are distinct from the arcuate anomaly close to Bond Nunatak. In total TDX anomaly margins enclose  $\sim 50$  per cent of the entire study area suggesting magnetic rocks are distributed throughout the study region.

The AGC filter of anomalies across Adelaide Island shows a similar pattern in the high frequency component to the pseudo gravity filter and TDX enhancement. This supports the suggestion that many of the magnetic sources defining the major trends in this region also have a relatively near-surface source component.

### 4.4 Apparent and measured susceptibility

Apparent susceptibility was calculated from the RTP data across Adelaide Island (Fig. 6d). Peak values of between  $15 \times 10^{-3}$  and  $35 \times 10^{-3}$  SI units were recovered from both the Northern and Southern Adelaide Island Surveys. Such susceptibilities would be most consistent with the mean measured susceptibility of gabbro on the AP ( $\sim 30 \times 10^{-3}$  SI units; Wendt *et al.* 2013). However, the

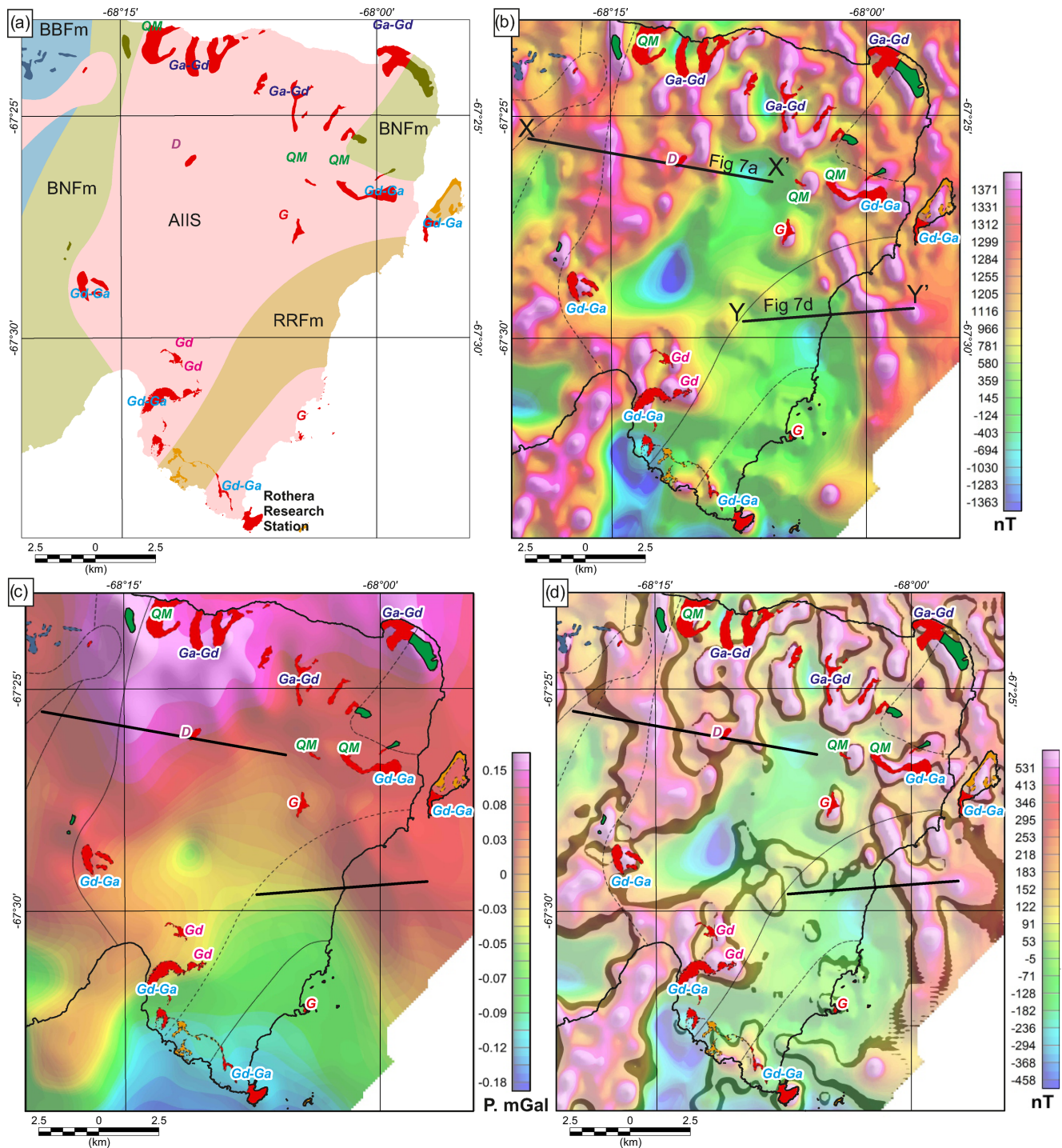


**Figure 5.** Detailed examination of Wright Peninsula. (a) Geological map. Coloured lettering marks different lithologies within the Adelaide Island Intrusive Suite (AIIS). QM, Quartz Monzonite; Ga-Gd, Gabbro-Granodiorite; D, Diorite; G, Gabbro; Gd, Granodiorite; Gd-Ga, Granodiorite-Gabbro. Black letters mark sedimentary or volcanic successions. BBFm, Buchia Buttress formation; BNFm, Bond Nunatak Formation; RRFm, Reptile Ridge Formation. Note extensive un-exposed AIIS rocks inferred across this area. (b) Automatic Gain Correction filter of magnetic data. Dashed lines and coloured areas represent inferred geological boundaries and observed rock outcrop from a. Black lines mark profiles in Fig. 7. Note contrasting northeast and northwest trending anomalies apparent across the region. Also note the lack of apparent sources in areas of little or no outcrop. (c) Pseudo gravity filter, accentuating longer wavelength anomalies, likely reflecting deeper magnetic sources. (d) TDX enhancement overlain on RTP magnetic data from Fig. 4. TDX values above 1.16 rad are coloured black to mark inferred anomaly boundaries. Note minor ‘ringing’ in this transform at the southeast edge of the survey area is an artefact.

maximum susceptibilities of almost all other igneous rock types on the AP exceed  $25 \times 10^{-3}$  SI units, making them possible sources. To further constrain the susceptibility of the local rocks on Adelaide Island, new susceptibility measurements were made on samples

from the Sillard Islands, Rigsby Island and Mt Vélain (Table 1). Sillard Islands diorites gave an average susceptibility of  $18.8 \times 10^{-3}$  SI units, similar to the tonalites and gabbros on offshore islands  $\sim 30$  km to the northeast (Wendt *et al.* 2013). Rigsby Island tonalites

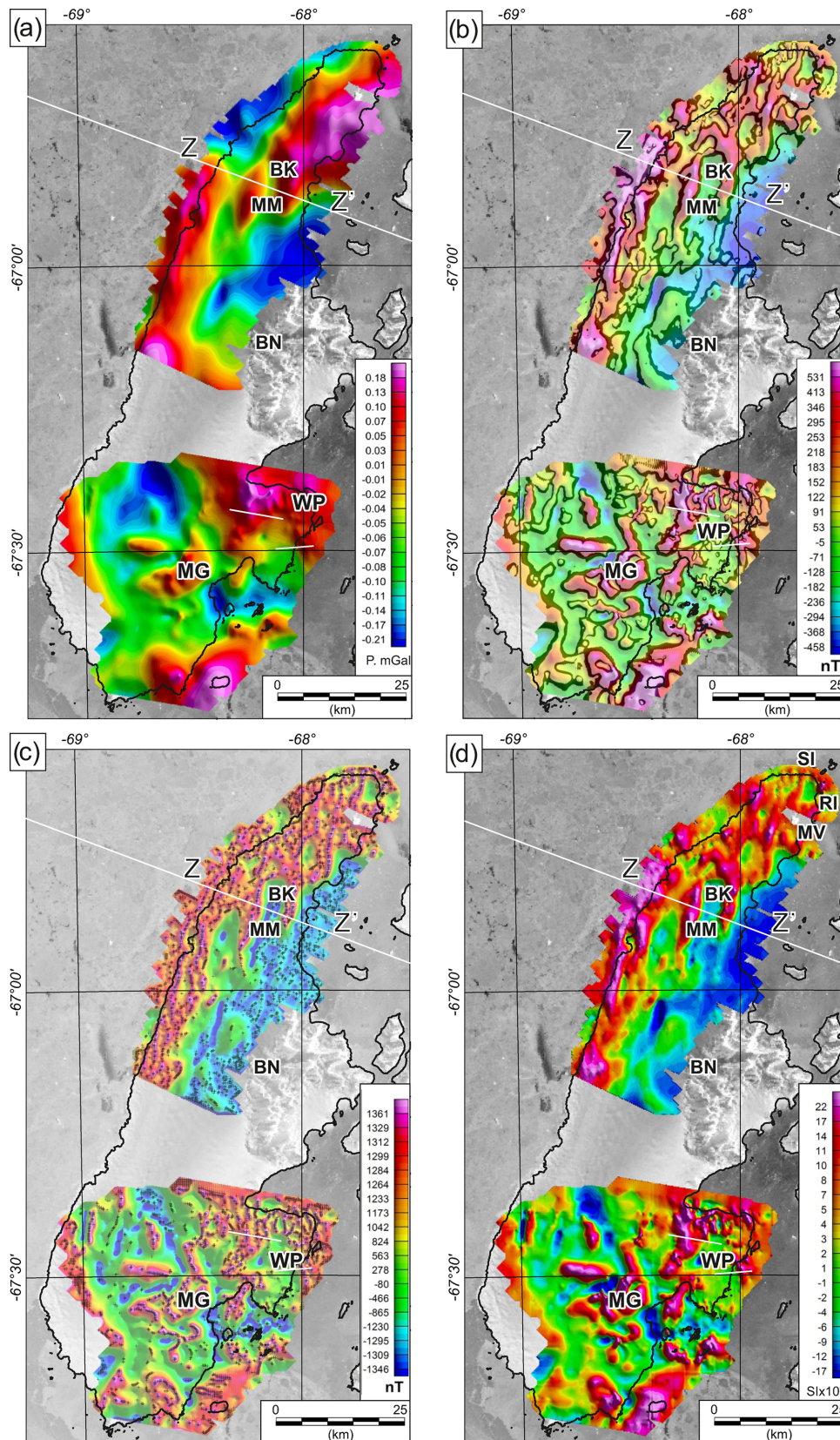


**Figure 6.** Digital enhancement across Adelaide Island. (a) Pseudo gravity. White lines mark modelled profiles. Note Z–Z' marks zoomed section in Figs 8(c)–(e). (b) TDX enhancement of anomaly margins (black >1.16 rad) overlain on RTP magnetic data. (c) AGC filter enhancement across Adelaide Island. Black crosses mark anomaly peaks used to create rose diagrams in Figs 10b and d. (d) Apparent susceptibility derived from RTP magnetic data.

**Table 1.** Magnetic susceptibility measurements from the Sillard Islands and Rigsby Island, and Mt Vélain made using a Terraplus™ KT-10 handheld magnetic susceptibility meter. Each value represents an average of three measurements of an individual rock sample now archived by the British Antarctic Survey collected in the 1950s (Goldring 1959; Goldring 1962) and 2006–2007. Samples marked with stars (\*) were dated.

Location	Sample no.	$\times 10^{-3}$ SI	Lithology
Sillard Islands	W339.1	10.7	Quartz diorite
Sillard Islands	W340.1	14.3	Quartz diorite
Sillard Islands	W340.2	12.8	Quartz diorite
Sillard Islands*	W341.1*	19.5	Quartz diorite
Sillard Islands	W342.1	48.9	Quartz diorite
Sillard Islands	W531.1	16.2	Quartz diorite
Sillard Islands	W532.2	17.8	Quartz diorite
Sillard Islands	W533.1	9.4	Quartz diorite
Sillard Islands	W533.2	19.3	Quartz diorite
Sillard Islands	W533.3	1.7	Meta sediment
Mt Vélain	J6.342.1	1.2	Fragmental volcanic breccia
Mt Vélain	J6.343.1	40.2	Basic dyke
Rigsby Island	W337.1	1.1	Tonalite
Rigsby Island	W336.2	0.6	Tonalite
Rigsby Island*	W336.1*	11.2	Tonalite
Rigsby Island	W336.1	25.8	Country rock

gave a lower average susceptibility ( $4.3 \times 10^{-3}$  SI units). However, a single sample of the adjacent fine grained dark igneous rock gave a susceptibility of  $25.8 \times 10^{-3}$  SI units. Two samples of Mt Vélain basalts had contrasting susceptibilities of  $1.2 \times 10^{-3}$  and  $40.2 \times 10^{-3}$  SI units consistent with the wide range of values noted for volcanic rocks elsewhere on Adelaide Island (Wendt *et al.* 2013).

## 5 MODELLING AND INVERSION

### 5.1 Wright Peninsula

2-D forward modelling and 3-D inversion of the aeromagnetic data was carried out to further constrain the subsurface structures across Adelaide Island. The 2-D models were calculated with the Geosoft™ GM-SYS software package. Our approach to the 2-D modelling was to use simple polygonal bodies to fit the form of the observed anomalies. We used peaks in the TDX field to help locate the margins of the modelled source bodies.

To further assess the structure of the region in 3-D we used the Geosoft™ VOXI inversion software (Bishop 2012). Due to the lack of subsurface control, and lack of information about the direction of magnetization, we ran an unconstrained inversion for source susceptibility, with a model volume extending to a depth of 8 km and bounded at the top by the ice surface. An iterative reweighting inversion focusing stage was applied to focus the results and sharpen the boundaries predicted by the initial inversion. A best fitting linear trend was removed from the input magnetic data prior to the 3-D inversion.

The first profile X–X' we modelled (Figs 7a–c) crossed a linear anomaly on the western edge of Wright Peninsula, and a nunatak where diorite crops out (Fig. 5b). Our initial 2-D model suggested the observed data (Fig. 7a) can be matched by two source bodies  $\sim 4$  km thick, with susceptibilities of  $41 \times 10^{-3}$  and  $23 \times 10^{-3}$  SI units, respectively (Fig. 7c). The boundaries of the higher susceptibility body were relatively well located by peaks in the TDX profile (Fig. 7b). However, the 2-D model for the edges of the lower susceptibility body does not agree as well with the TDX peaks. From

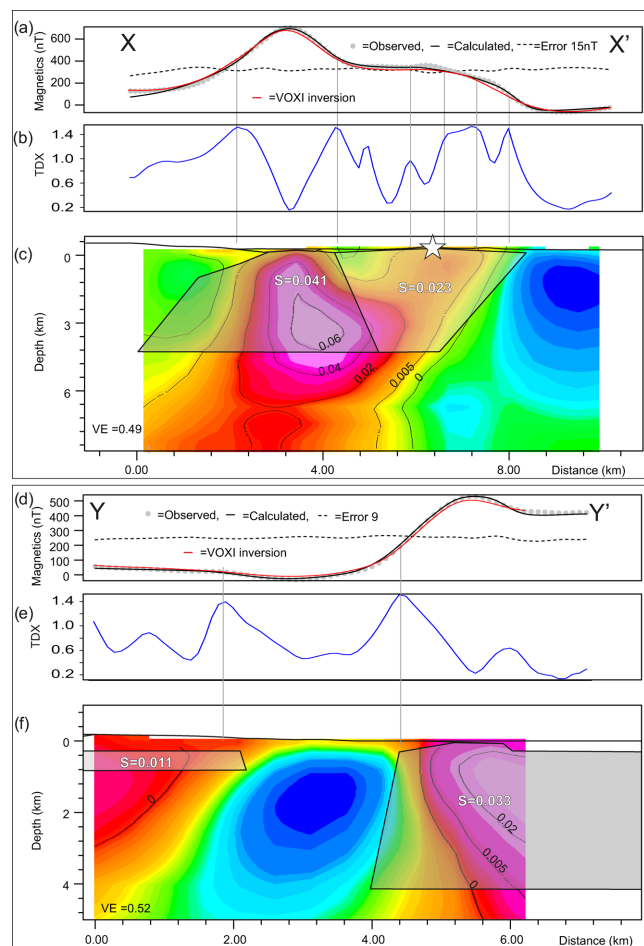


**Figure 7.** 2-D models of magnetic anomalies on Wright Peninsula, located on Fig. 5. (a) Observed and calculated magnetic anomaly field from both 2-D forward model and 3-D VOXI inversion on the northern Wright Peninsula model. (b) TDX profile. Vertical grey lines mark TDX peaks. (c) Model structure. Semi-transparent grey polygons, and white text define 2-D forward model. Coloured background image shows susceptibility sampled from the result of our VOXI 3-D inversion. Thin black lines mark susceptibility contours labelled in black. Note negative values are not contoured. All susceptibility units are SI units. White star locates diorite outcrop. Vertical exaggeration (VE) is marked in the lower left corner of the model. (d) Observed and calculated magnetic anomalies along the southern Wright Peninsula model. (e) TDX enhancement. (f) 2-D forward model (polygons) and VOXI 3-D susceptibility inversion (coloured section).

the map view of Wright Peninsula (Fig. 5b) it is apparent that this lower amplitude part of the anomaly is likely contaminated by more complex 3-D effects, not considered in the 2-D model.

To compare our 2-D forward modelling results with the 3-D VOXI inversion we extracted a coincident section from the inversion results (Fig. 7c). The 3-D inversion suggests that the observed anomaly can be accounted for by a high susceptibility body (over  $60 \times 10^{-3}$  SI units), with a subsidiary branch with lower susceptibility extending towards the outcrop of diorite. The source body boundaries are not clearly defined in the 3-D VOXI model. Nevertheless, a threshold value of  $5 \times 10^{-3}$  SI units gives a body with margins close to those predicted by the TDX analysis, and approximately agree with the bodies from the 2-D forward models. One problem with the 3-D inversion is that negative susceptibilities are predicted. These may reflect areas of remnant magnetization, or simply problems with the use of a poorly constrained inversion. As we

have no way to better constrain the 3-D inversion we assume these features are artefacts, and that only features with a susceptibility  $> 5 \times 10^{-3}$  SI units reflect real geological bodies.

The second profile on Wright Peninsula we analysed (Y–Y'); Figs 7d–f) crosses a narrow linear anomaly on the eastern edge of the survey area (Fig. 5b). Our 2-D model shows that this anomaly can be accounted for by a body  $\sim 4$  km thick with a susceptibility of  $33 \times 10^{-3}$  SI units. It was found that an additional shallow body with relatively low susceptibility was required at the opposite end of the section to create the observed inflection. The margin of this body approximately correlates with a peak in TDX. The 3-D inversion showed a similar pattern to our 2-D model, with high susceptibilities beneath the main anomaly. However, the dip of the source body defined by the 2-D model and 3-D inversion has an opposite sense (Fig. 7f). Given the steep dip derived from both techniques ( $\sim 84^\circ$ ) we do not believe the true dip direction is resolved by either method. The susceptibilities and body thicknesses required for both modelled profiles across Wright Peninsula (Figs 7c and f) are similar suggesting that this type of source geometry is typical of the region.

## 5.2 The Northern Adelaide Island survey area

To investigate the structure of the subsurface geology in the Northern Adelaide Island Survey area, we followed a two-step approach for the 2-D modelling, as our local data is influenced by a strong regional trend. We first modelled the regional magnetic anomaly along a profile extending  $\sim 95$  km westwards offshore from Adelaide Island, and  $\sim 75$  km eastwards onshore onto the AP (Figs 8a and b). The bodies from this regional model were then input as the starting point for our local model of the high resolution data collected by the Northern Adelaide Island Survey (Figs 8c–e).

To fit the reconnaissance magnetic data (Fig. 8a) two highly magnetic batholiths up to  $\sim 12$  km thick were required, separated by an intervening basin  $> 5$  km deep (Fig. 8b). Our model suggests that these bodies may be joined at depth. This regional model is similar to that of previous authors who suggested the magnetic AP Pacific margin batholiths had high susceptibility and were up to 20 km thick (Garrett 1990; Johnson 1999).

Our local 2-D model of the Northern Adelaide Island aeromagnetic data included the deeper body from the regional model, and was further constrained by the predicted location of source body margins from TDX calculation (Figs 8c and d). In addition we chose a profile which intersects Mt Machatschek, where rocks of the AIIS have been recognized. Our best fitting 2-D model required three additional bodies extending from the surface to a depth of  $\sim 4$  km. The required susceptibility of these bodies was between 16 and  $60 \times 10^{-3}$  SI units. Two of these bodies appear to extend to the top of the underlying body derived from the regional model. Although the main body from the regional model was retained, removing the link to the AP batholith improved the fit of the data at the right-hand margin of the model.

The 3-D inversion across the Northern Adelaide Island Survey also recovers three main shallow source bodies along this profile (Fig. 8e). The inversion suggests two of the bodies extend to a depth of  $\sim 3$  km, assuming a threshold of  $5 \times 10^{-3}$  SI units. This threshold gives rise to sources with margins in reasonable agreement with the predictions of the TDX enhancement and our independent 2-D forward model. The 3-D model does not predict a deeper source extending beneath the region as the high resolution survey does not resolve this structure, and a linear trend was removed from the data before inversion was carried out.

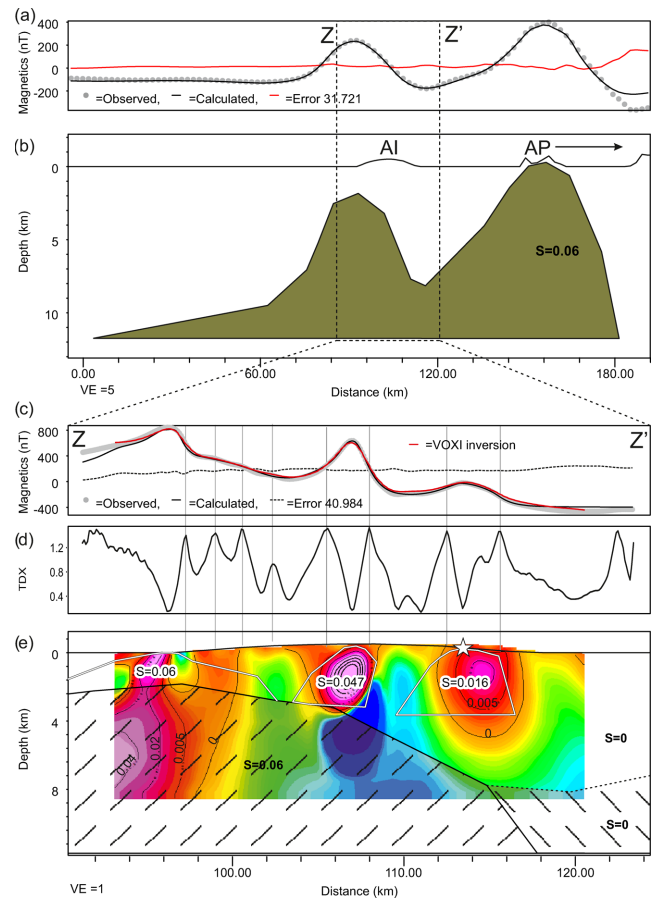


**Figure 8.** Model across the Northern Adelaide Island Survey. (a) Regional aeromagnetic anomaly data from ADMAP, and output from 2-D model. (b) Subsurface geological bodies required to match regional data in a. AI Adelaide Island, AP Antarctic Peninsula. (c) Zoom on profile Z–Z' across the Northern Adelaide Island Survey, showing high resolution aeromagnetic data, 2-D modelling and 3-D inversion results. (d) TDX peak values from high resolution data. (e) Modelled susceptibility structure. Black outlined polygons with dashed fill mark deep bodies from b. White outlined polygons required to fit our new high resolution aeromagnetic data in 2-D. Note susceptibility of the right hand deep body is set to zero to improve the fit to the high resolution data. White star marks inferred AIIS outcrop at Mt Machatschek. Background coloured image shows the output of the 3-D VOXI inversion along this profile. Note good correspondence with results of independent 2-D forward modelling of shallow structures.

## 5.3 3-D inversion and upper crustal magnetic source volume

To calculate the 3-D form and volume of the magnetic source bodies within our study region we applied a threshold to our VOXI inversion results of  $5 \times 10^{-3}$  SI units (Fig. 9). This threshold was chosen as it gave bodies with margins approximately matching the TDX estimates. The average susceptibility for all sources above our imposed threshold was  $\sim 22 \times 10^{-3}$  SI units. This average susceptibility is consistent with the results of apparent susceptibility calculation (Fig. 6d), direct susceptibility measurements on the Sillard Islands, and our 2-D forward models (Figs 7 and 8), suggesting that  $5 \times 10^{-3}$  SI units is an appropriate threshold. However, the resulting volumes we calculate only reflect magnetic sources within the modelled upper 8 km of the crust, as this was the limit of our model, and our high-resolution surveys do not fully sample the longer wavelength anomalies required to help determine the

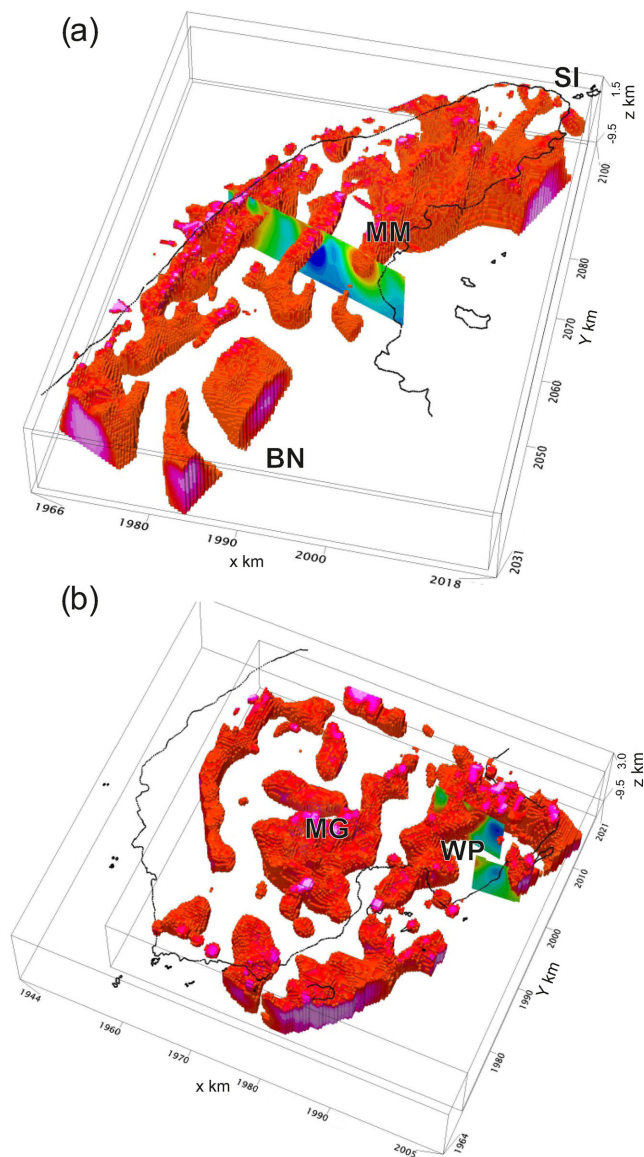


**Figure 9.** 3-D view of magnetic source bodies from VOXI 3-D inversion. (a) Inversion result across the Northern Adelaide Island Survey. Only cells with susceptibility  $>0.005$  SI units are shown. Cross section close to Mt Machatschek (MM) marks Fig. 8e. (b) Inversion results across the Southern Adelaide Island Survey. Note cross sections on Wright Peninsula (WP) from Fig. 7, and separate source body beneath Mt Gaudry (MG).

volume of deeper structures. Additionally, our calculations can only provide a guide to the true intrusive volume, as our inversion had limited constraints, and different susceptibility thresholds will give different intrusive volumes.

Across the Northern Adelaide Island Survey area the sources of the linear anomalies are generally well resolved by the 3-D inversion as linear bodies 3–5 km thick (Fig. 9a) that lie totally within the model space. The linear bodies generally extend from a thicker body; however, the inversion did not resolve the base of these thicker sources, implying their base is deeper than the 8 km assumed thickness of the inversion space, increasing the uncertainty of the recovered source volume. In total the inversion suggests that magnetic sources in the Northern Adelaide Island Survey area account for  $\sim 3500$  km<sup>3</sup> of material, which is  $\sim 26$  per cent of the volume within the model domain ( $<8$  km depth). In the Southern Adelaide

Island Survey area the inversion suggests that separate source bodies are present beneath Wright Peninsula and Mt Gaudry, with no clear trend being apparent in the subsurface structures. In total the magnetic bodies in the Southern Adelaide Island Survey area have a predicted volume of  $\sim 4000$  km<sup>3</sup>, which is  $\sim 23$  per cent of the volume within the model domain.

## 6 INTERPRETATION

### 6.1 Sources of magnetic anomalies on Adelaide Island

The high amplitude magnetic anomalies on Wright Peninsula are spatially coincident with outcrops of granodiorite and gabbroic rocks of the AIIS (Fig. 5). This correlation is seen across other parts of Southern Adelaide Island (Fig. 10a). We therefore propose that the main sources for the magnetic anomalies across Southern Adelaide Island are AIIS rocks. Our 3-D inversion suggests that Southern Adelaide Island contains at least two separate plutons,  $>4$  km thick and  $\sim 10$  km across beneath Wright Peninsula and Mt Gaudry. In total our inversion suggests these intrusive rocks form  $\sim 23$  per cent of crust shallower than 8 km (Fig. 9b). This is approximately consistent with geological mapping (Fig. 2), which shows that across Adelaide Island  $\sim 56$  per cent of all outcrops are igneous rocks, with an inferred extent covering  $\sim 33$  per cent of the study area. The AIIS rocks generally appear to be highly magnetic irrespective of their classification (tonalite, gabbro or granodiorite) suggesting magnetite is abundant in all these rock types. This would be consistent with the intrusions on Southern Adelaide Island being dominantly arc rocks, sourced from a hydrated and oxidized mantle wedge (Wendt *et al.* 2013).

Across Northern Adelaide Island, sparse outcrop makes interpretation of the magnetic sources problematic. The source geometry is different to that observed further south, with clear indications of structural control of the sources (Fig. 10a). Exposed AIIS rocks are coincident with a linear anomaly at Blümcke Knoll, are inferred from more distant observations at Mt Machatschek (Dewar 1962), and are extensively exposed on the Sillard Islands, just to the north of the survey area. We therefore propose that structurally controlled AIIS rocks are the source for the observed linear anomalies across Northern Adelaide Island. Additionally, we suggest that all the north–northeast orientated linear anomalies along the western edge of Adelaide Island represent a continuation of these structurally controlled intrusions (Fig. 10a). The structural control of the intrusions in Northern Adelaide Island implies emplacement in a different geodynamic setting, or exposure of a different crustal level, to those across Southern Adelaide Island. The presence of ‘flow banding’ on the Sillard Islands and Blümcke Knoll (Dewar 1962; Goldring 1962), not observed further south on Adelaide Island, can be argued as evidence for a distinct emplacement setting for the northern structurally controlled intrusions.

### 6.2 Age of emplacement

Across Southern Adelaide Island multiple dates suggest a Palaeogene age for the exposed intrusions (Griffiths & Oglethorpe 1998; Riley *et al.* 2012). We extrapolate this to interpret all the intrusions which show little structural control in our aeromagnetic data across Southern Adelaide Island to be Palaeogene (Fig. 10a). The most northerly Palaeogene date comes from Mt Bouvier. We interpret the arcuate magnetic anomaly to the north of Mt Bouvier as reflecting the continuation of the Palaeogene Mt Bouvier pluton, which

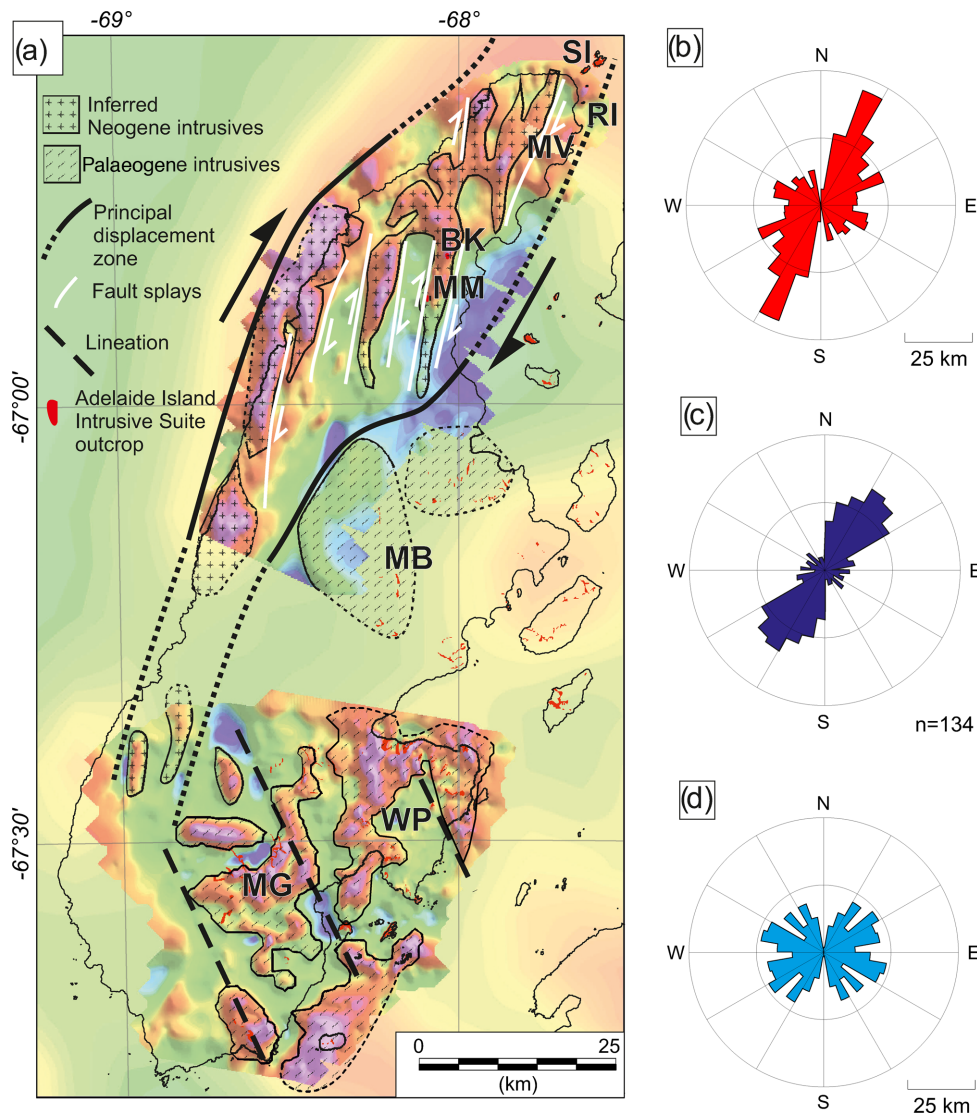


**Figure 10.** Structural and geological interpretation. (a) Aeromagnetic anomaly map with geological interpretation. Thick solid and dotted black lines mark inferred Neogene dextral transtensional fault system, white lines mark inferred fault splays. Thick dashed black lines mark lineations associated with Palaeogene motion across Marguerite Bay to the south. Thin solid and dashed black lines mark interpreted and extrapolated intrusion margins respectively. Dated Neogene and Jurassic rocks are from the Sillard (SI) and Rigsby (RI) islands respectively. (b) Cumulative lineation length and orientation derived from peaks along AGC filtered anomalies in the Northern Adelaide Island Survey. (c) Radial plot of 134 late stage dyke strike directions (Riley *et al.* 2012). (d) Cumulative lineation length and orientation from peaks along AGC lineations in the Southern Adelaide Island Survey.

geological mapping shows is exposed just  $\sim 2$  km from the northern survey area (Fig. 10a).

Our new dating of intrusive rocks to the Neogene on the Sillard Islands ( $\sim 23$  Ma), and the Jurassic on Rigsby Island ( $\sim 156$  Ma) gives contrasting possible ages for the structurally controlled intrusions across the northern and western edges of Adelaide Island. We prefer a younger Neogene age for the proposed intrusions. The higher average susceptibility of AIIS rocks on the Sillard Islands, compared to Rigsby Island, is consistent with the younger AIIS rocks as the source of the observed magnetic anomalies, but cannot be considered diagnostic. The trend of the structurally controlled intrusions, inferred from the magnetic data (Fig. 10b), is similar to the trend of the late stage dykes (Fig. 10c), which cross-cut all other lithologies further south on Adelaide Island (Riley *et al.* 2012). Although we cannot image the dykes in our aeromagnetic data across Southern Adelaide Island, they demonstrate that a late-stage north–northeast orientated phase of magmatism occurred, consistent with

a younger (Neogene?) age for the structurally controlled intrusions to the northwest. On the Sillard Islands, AIIS rocks have an intrusive contact with thermally metamorphosed volcanic rocks, which, to the south at Mt Velain, are mapped as Late Cretaceous in age (Riley *et al.* 2012), providing further indirect evidence for a post-Cretaceous age for the intrusions. Additionally, a sliver of Jurassic arc outboard of the Jurassic forearc sediments mapped in the central and southern part of Adelaide Island (Fig. 2) would require complex later faulting, similar to that which moved tectonic fragments along branches of the San Andreas fault system in California (Ponce *et al.* 2004). Such complex faulting cannot be ruled out from our data, and would explain the Jurassic magmatic rocks on Rigsby Island; however, later stage Neogene magmatism seems a simpler explanation for the interpreted en echelon pattern of intrusions outboard of the Jurassic forearc. Although we do not think the inferred structurally controlled intrusions are Jurassic in age the presence of Jurassic rocks on Rigsby Island is consistent with the presence of Jurassic

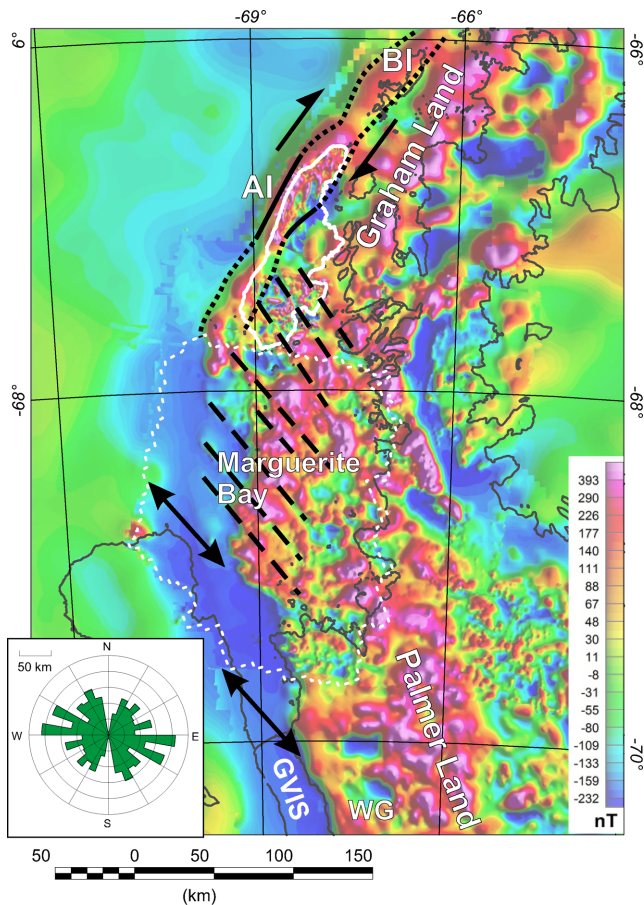


**Figure 11.** Composite regional aeromagnetic anomaly map including data from previous workers (Johnson 1999; Golynsky *et al.* 2001; Ferraccioli *et al.* 2006) and our new data. Inset shows cumulative lineation length for the area of Marguerite Bay outlined by dotted white line. Solid white outlines mark Adelaide Island. Thick solid and dotted black lines mark inferred Neogene dextral shear zone making up western strand of the Pacific Margin Anomaly (PMA) extending 30–100 km NE from Adelaide Island (AI) to the Bisco Islands (BI). Thick dashed lines mark lineations on Southern Adelaide Island, and previously noted across Marguerite Bay (Johnson 1997). Black arrows show Palaeogene to Neogene inferred extension direction along George VI Sound and across Marguerite Bay (Johnson 1997). Note apparent truncation of Marguerite Bay lineations against inferred Neogene shear zone.

arc basement mapped and dated further inboard along the Antarctic Peninsula southeast of Adelaide Island (Leat *et al.* 2009).

### 6.3 Kinematic setting

Magnetic lineament analysis alone does not provide definitive structural geological interpretations or kinematic solutions (Betts *et al.* 2003; Ferraccioli & Bozzo 2003). However, the pattern of intrusions across Adelaide Island can be interpreted in terms of the kinematics of the AP as a whole. Southern Adelaide Island shows a complex range of lineation orientations (Fig. 10d), including northwest trending structures, which cut both the Wright Peninsula and Mt Gaudry (Fig. 10a). Analysis of the magnetic fabric to the south, across Marguerite Bay, reveals a similar complex pattern of lineations, including a number of northwest trending structures (Fig. 11).

In Marguerite Bay the northwest orientation of the magnetic lineations, marking the Transition Zone between Graham Land and Palmer Land sections of the AP, has previously been linked with

continental interaction with oceanic transform features (Garrett 1990; Noltimier 1998; Johnson 1999). One model for the magnetic lineations is that they reflect left lateral displacement of the AP to the northwest (Garrett 1990). This view is supported by analysis of trends visible in satellite imagery and interpreted to reflect a sinistral Riedel shear system (Noltimier 1998). An alternative model for the lineations in Marguerite Bay is that they reflect faults associated with dextral transtensional opening of George VI Sound from 50 to 30 Ma, with extension potentially continuing in Marguerite Bay until ~20 Ma (Johnson 1997). Extension is linked with Palaeogene slowdown, and ultimately cessation of subduction outboard of Alexander Island and Marguerite Bay (Johnson 1997). Regionally the extensional opening of George VI Sound has been linked with Cenozoic extension in the West Antarctic Rift System (Eagles *et al.* 2009b; Jordan *et al.* 2010; Bingham *et al.* 2012). The north westerly trending lineations on Southern Adelaide Island lead us to interpret this area kinematically as a continuation of the Marguerite Bay region. Although we cannot differentiate between the proposed dextral or sinistral models for Marguerite Bay, the dating of the intrusions on Adelaide Island is consistent with Palaeogene movement.

Across Northern Adelaide Island, a different structural/kinematic setting to Marguerite Bay is revealed by a distinct pattern of en echelon intrusions (Figs 10a and b). Given the relatively large volume of emplaced material suggested by our 3-D inversion (~25 per cent of the upper crust) a dominantly extensional or transtensional environment is envisaged to create the required accommodation space. We suggest that the en echelon pattern of intrusion would be most consistent with transtension. Given the geometry of the inferred intrusions, which appear to step to the right, around the Palaeogene Mt Bouvier pluton, a dextral strike-slip setting would create transtension, whereas a sinistral strike-slip setting would create transpression. Our preferred interpretation is therefore that the north-northeast trending structures reflect magma emplacement within an extensional duplex in a major dextral fault system (Woodcock & Fischer 1986) with a northeast trending principal displacement zone (Fig. 10a). In this model the individual linear intrusions are emplaced along dextral fault splays in a 'leaky' releasing bend within an overall transtensional fault system. The two offset deeper bodies imaged by the pseudo gravity filter (Fig. 6a) either side of the narrow en echelon intrusions reflect the regional continuation of the transtensional fault system. An alternative interpretation invokes oblique east–west extension, with the linear intrusions emplaced on a series of normal faults, or along right-stepping relays in an extensional fault system. However, an extensional model does not account as well for the observed en echelon pattern of intrusion.

Regionally the en echelon intrusions we image across northern Adelaide Island correlate with a ~30 km wavelength north-east trending anomaly extending from Adelaide Island to the Bisco Islands ~75 km to the northeast (Fig. 11). Our modelling (Fig. 8) leads us to interpret this regional structure as a deeper batholith in agreement with previous authors (Garrett 1990; Johnson 1999). It is not possible from our magnetic data alone to tell if the shallow en echelon intrusions are part of this deeper batholith. However, on the Bisco Islands the observed positive magnetic anomaly correlates with exposed, high susceptibility tonalites and gabbros (Smellie *et al.* 1985; Wendt *et al.* 2013), supporting the interpretation that the deeper batholith extends to the surface. We therefore suggest that the shallow, structurally controlled Neogene intrusions we infer on Northern Adelaide Island are part of the underlying batholith, which extends ~200 km along the western margin of the AP from southern Adelaide Island to the Bisco Islands to the north. The apparent

truncation of the Early to mid Cenozoic Marguerite Bay structures (Fig. 11) by the linear northeast trending marginal anomaly would also support a younger Cenozoic age for the linear anomalies. Alternatively the regional northeast trending anomaly may reflect an older, unexposed arc basement structure which, on Adelaide Island, has been exploited by a younger phase of magmatism. Further dating of the intrusions on the Bisco Islands would reveal the full extent of the shallow Neogene intrusions in this region.

## 7 DISCUSSION

### 7.1 Implications of extensive Cenozoic magmatism

Our interpretation that the western branch of the PMA on Adelaide Island is due to Cenozoic arc related intrusions has significant implications for understanding the evolution of the AP arc. 3-D inversion suggests that around 25 per cent of the upper 8 km of the crust may be composed of 4–6-km-thick Cenozoic intrusions (Fig. 9). This is consistent with the widespread geological mapping of Palaeogene AIIIS rocks across Southern Adelaide Island. Additionally our model of regional aeromagnetic data suggests the Neogene intrusions may be part of a larger batholith, over 10 km thick (Fig. 8b). The volume of magma emplaced would imply that arc magmatism did not decline very significantly into the Cenozoic, as suggested previously (Leat *et al.* 1995), rather the locus of magmatism moved towards the western edge of the arc, and the resulting intrusions are today poorly exposed. The significant volumes of magmatism we model suggest that there is a distinct western branch of the PMA extending northward from Adelaide Island, separate from the eastern strand of the PMA on the Antarctic Peninsula, where predominantly Jurassic and Cretaceous ages have been found (Leat *et al.* 1995). This supports the original proposal that the PMA is a composite structure (Garrett 1990), rather than a single Cretaceous feature, as suggested for the southern part of the AP (Vaughan *et al.* 1998).

The recognition that different strands of the PMA may reflect different ages of arc magmatism implies the strands of the PMA could be primary features, reflecting separate positions for the magmatic focus, rather than the result of Cenozoic splitting of the arc, as favoured by some previous authors (Johnson 1999). However, along Bransfield Strait, at the northern tip of the AP the arc batholiths have clearly been split by Cenozoic extension (Larter & Barker 1991). However, we suggest that this rift may have exploited a pre-existing boundary between two separate magmatic domains.

### 7.2 Driving mantle process

The presence of proposed distinct Neogene, structurally controlled arc intrusions along the western edge of the AP raises the question of what process triggered magmatism at this time. We suggest that the cessation of subduction south of Adelaide Island ~30 Ma played a key role (Fig. 12). As the subducted plate south of Adelaide Island foundered into the asthenosphere a slab window would have opened (Hole *et al.* 1991). Models have shown that opening of such a slab window would allow enhanced mantle return flow around the still subducting plate and facilitate enhanced slab roll-back (Fig. 12; Kincaid & Griffiths 2003; Piromallo *et al.* 2006; Schellart *et al.* 2007). Slab roll-back can cause trench normal extension, within the overriding arc, in an oblique extensional, or transtensional kinematic setting. This would facilitate emplacement of large volumes of magma, as seen for example along the Nicaraguan arc (Morgan *et al.* 2008). Additionally, lateral transport of more fertile juvenile

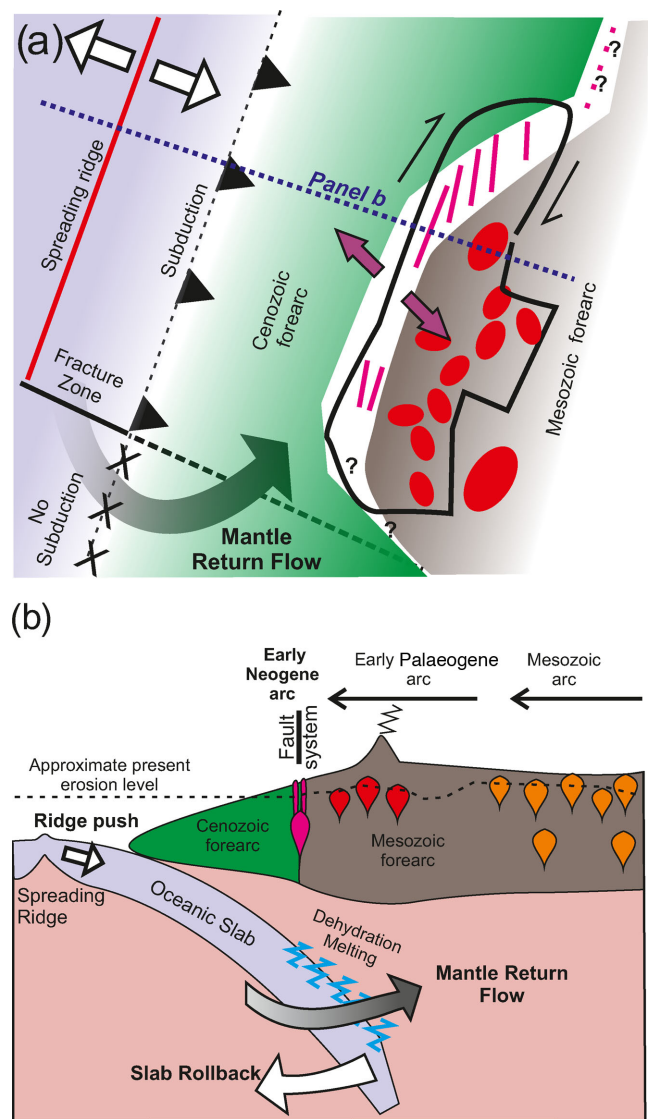


**Figure 12.** Cartoon showing possible impact of cessation of subduction and opening of a slab window south of Adelaide Island. (a) Map of Neogene tectonic setting of Adelaide Island, outlined in black. Mantle flow (thick grey arrow) loops around the end of the still subducting plate, enhancing slab roll back. Suggested Neogene magmatism (pink) is then focused along the boundary between the Palaeogene arc (red intrusions) and the forearc (green). This boundary acts as a structural discontinuity, along which the Neogene Fault system develops (white region). The Palaeogene arc itself intrudes the older Mesozoic forearc (brown), while the older Mesozoic intrusions (orange) lie further inboard. (b) Cross section through same system, showing proposed dextral Neogene fault system along arc/forearc boundary.

mantle material into the mantle wedge may lead to enhanced magma generation, as proposed for Mt Etna in southern Italy (Dogliani *et al.* 2001). This mechanism of lateral mantle flow through a slab window has been suggested as a driving mechanism for backarc extension along the Bransfield Strait part of the AP, due to subduction of the spreading centre south of the Hero Fracture Zone (Barker & Austin Jr 1998). The northern termination of the Tonga arc, and extending Lau Basin is a further example where geochemical (Turner & Hawkesworth 1998), geodynamic (Bevis *et al.* 1994) and seismic (Smith *et al.* 2001) data together demonstrates that lateral mantle flow is facilitating slab roll-back and extension in the upper plate, now focused on the Lau backarc basin.

We hypothesize that together the processes of slab roll back and rejuvenation of the mantle, triggered by opening of a slab window south of Adelaide Island, drove the formation and emplacement of the structurally controlled Neogene arc magmas we infer along the western edge of Adelaide Island. The amount of extension we envisage is on a smaller scale to the development of back-arc basins proposed in other areas. However, we suggest that the changing mantle dynamics accompanying cessation of subduction, within 10 Ma of the inferred magmatism, is a likely significant factor accounting for the distinct structurally controlled Neogene magmas. Our tentative correlation of exposed intrusions on the Bisco Islands as part of the same magmatic structure, suggests that this mantle process could have affected over 200 km of the AP margin.

Slab window formation along the AP is a geometric necessity because the oceanic crust outboard of the spreading centre is part of the Antarctic Plate (Larter & Barker 1991; McCarron & Larter 1998). Evidence that slab windows formed along the AP comes from geochemical analysis of back arc volcanoes and intrusions (Hole & Larter 1993; McCarron & Smellie 1998) and plate modelling (Eagles *et al.* 2009a). Additionally, low-temperature thermochronology reveals uplift and exhumation at 10–15 Ma linked with development of a slab-window beneath the Adelaide Island/Bisco Island region (Guenther *et al.* 2010). The process we propose is distinct from the post-subduction slab-window magmatism already suggested for the AP (McCarron & Larter 1998), in which the slab has been removed, and magmatism is no longer driven by dehydration of a downgoing slab. In the model we propose magmatism is continuing above a subducting slab (Fig. 12b).

Our hypothesis that changing mantle flow drove structurally controlled Neogene magmatism along the Graham Land sector of the AP could be tested in a number of ways. Firstly future high resolution aeromagnetic surveys across Adelaide Island would confirm if the linear structures from the Northern Adelaide Island Survey continue along the west coast of Adelaide Island, and help to better constrain the boundary between the more and less structurally controlled parts of the arc. Secondly detailed aeromagnetic surveys across the arc/forearc boundary to the north of Adelaide Island would confirm the link with AIIS rock outcrops on the Sillard Islands, and the Bisco Islands 30–100 km to the north. Further dating of rock samples from the Bisco Islands would confirm or refute the hypothesis that extensive Neogene magmatism occurred along the margin of the AP, and geochemical analysis could test for the presence of mantle flow through the slab window.

## 8 CONCLUSIONS

High resolution aeromagnetic surveys across Adelaide Island west of the Antarctic Peninsula reveal the structure and extent of Cenozoic magmatism along the arc/forearc boundary. In this region 3–5-km-thick Palaeogene and Neogene Plutons make up around 25 per cent of the upper crust. This highlights the important and long lived process of magma emplacement forming the magnetic PMA along the Antarctic Peninsula.

Evidence for a high degree of structural control over the outboard parts of the arc is imaged by high resolution aeromagnetic surveys of Adelaide Island. We argue that this reflects an increase in the degree of structural control on magma emplacement in Neogene times.

A mantle process, previously unrecognized on this part of the Antarctic Peninsula, is proposed to account for the Neogene structures we infer. Cessation of subduction further south along the arc

at ~30 Ma triggered opening of a slab window, enhanced mantle return flow and slab roll back. This in turn generated the observed structurally controlled magmatism, which appears to have preferentially focused along the arc/forearc boundary. We suggest that this process in part explains the western most strand of the PMA extending at least 200 km along the northern part of the Antarctic Peninsula.

## ACKNOWLEDGEMENTS

This work was funded by NERC British Antarctic Survey core funds as part of the Polar Science for Planet Earth programme. We wish to thank the staff at Rothera Research Station for logistical support, and Carl Robinson our survey engineer for technical assistance. We also wish to thank P. East, K. Gardner, Prof Fairhead and Dr Green from GETECH Group plc and Leeds University for assistance with processing the Northern Adelaide Island airborne magnetic data. Kerstin Lindén and Lev Ilyinsky are thanked for their assistance at the NORDSIM facility. This is NORDSIM publication number 372.

## REFERENCES

- Barker, D.H.N. & Austin, J.A. Jr, 1998. Rift propagation, detachment faulting, and associated magmatism in Bransfield Strait, Antarctic Peninsula, *J. geophys. Res.*, **103**, 24 017–24 043.
- Betts, P.G., Giles, D. & Lister, G.S., 2003. Tectonic environment of shale-hosted massive sulphide Pb-Zn-Ag deposits of Proterozoic northeastern Australia, *Econ. Geol.*, **98**, 557–576.
- Bevis, M. *et al.*, 1994. Geodetic observations of very rapid convergence and back-arc extension at the Tonga arc, *Nature*, **374**, 249–251.
- Bingham, R.G., Ferraccioli, F., King, E.C., Larter, R.D., Pritchard, H.D., Smith, A. & Vaughan, D.G., 2012. Inland thinning of West Antarctic Ice Sheet steered along subglacial rifts, *Nature*, **487**, 468–471.
- Bishop, C., 2012. Interpretation and Modelling of the Pedirka Basin (central Australia) using Magnetics, Gravity, Well-log and Seismic data, in *Proceedings of the 22nd International Geophysical Conference and Exhibition*, Brisbane, Australia.
- Blakely, R.J. & Simpson, R.W., 1986. Approximating edges of source bodies from magnetic or gravity anomalies, *Geophysics*, **51**, 1494–1498.
- Cook, A.J., Murray, T., Luckman, A., Vaughan, D.G. & Barrand, N.E., 2012. A new 100m Digital Elevation Model of the Antarctic Peninsula derived from ASTER Global DEM: methods and accuracy assessment, *Earth Syst. Sci. Data*, **4**, 129–142.
- Cooper, G.R.J. & Cowan, D.R., 2006. Enhancing potential field data using filters based on the local phase, *Comput. Geosci.*, **32**, 1585–1591.
- Cordell, L.E. & Grauch, V.J.S., 1985. Mapping basement magnetization zones from aeromagnetic data in the San Juan Basin, New Mexico, in *The Utility of Regional Gravity and Magnetic Anomaly Maps*, pp. 181–197, ed. Hinze, W.J., Soc. Explor. Geophys.
- De Ritis, R.R.D., Ventura, G., Nicolosi, I., Chiappini, M., Speranza, F., De Rosa, R., Donato, P. & Sonnino, M., 2010. A buried volcano in the Calabrian Arc (Italy) revealed by high resolution aeromagnetic data, *J. geophys. Res.*, **115**, doi:10.1029/2009JB007171.
- Dewar, G.J., 1962. Unpublished field notebook, British Antarctic Survey Archives (ES3/GY33/2.1/9).
- Dewar, G.J., 1970. The geology of Adelaide Island. British Antarctic Survey Scientific Reports, *Br. Antarctic Surv. Scient. Rep.*, **57**, 1–66.
- Doglioni, C., Innocenti, F. & Mariotti, G., 2001. Why Mt Etna?, *Terra Nova*, **13**, 25–31.
- Eagles, G., Gohl, K. & Larter, R.D., 2009a. Animated tectonic reconstruction of the Southern Pacific and alkaline volcanism at its convergent margins since Eocene times, *Tectonophysics*, **464**, 21–29.

- Eagles, G., Larter, R.D., Gohl, K. & Vaughan, A.P.M., 2009b. West Antarctic Rift System in the Antarctic Peninsula, *Geophys. Res. Lett.*, **36**, doi:10.1029/2009GL040721.
- Ferraccioli, F. & Bozzo, E., 2003. Cenozoic strike-slip faulting from the eastern margin of the Wilkes Subglacial Basin to the western margin of the Ross Sea Rift: an aeromagnetic connection, in *Intraplate Strike-Slip Deformation Belts*, pp. 109–133, eds Storti, F., Holdsworth, R.E. & Salvini, F., The Geological Society of London Special Publication.
- Ferraccioli, F., Gambetta, M. & Bozzo, E., 1998. Microlevelling procedures applied to regional aeromagnetic data: an example from the Transantarctic Mountains (Antarctica), *Geophys. Prospect.*, **46**, 177–196.
- Ferraccioli, F., Jones, P.C., Curtis, M.L., Leat, P.T. & Riley, T.R., 2005. Tectonic and magmatic patterns in the Jutulstraumen rift(?) region, East Antarctica, as imaged by high-resolution aeromagnetic data, *Earth Planets Space*, **57**, 767–780.
- Ferraccioli, F., Jones, P.C., Vaughan, A.P.M. & Leat, P.T., 2006. New aerogeophysical view of the Antarctic Peninsula: More pieces, less puzzle, *Geophys. Res. Lett.*, **33**, doi:10.1029/2005GL024636.
- Ferraccioli, F. *et al.*, 2007. Collaborative aerogeophysical campaign targets the Wilkes Subglacial Basin, the Transantarctic Mountains and the Dome C region, in *The Italian–British Antarctic Geophysical and Geological Survey in Northern Victoria Land 2005–06–Towards the International Polar Year 2007–08*, pp. 1–36, eds Bozzo, E. & Ferraccioli, F. *et al.*, Terra Antarctica Reports.
- Garrett, S.W., 1990. Interpretation of reconnaissance gravity and aeromagnetic surveys of the Antarctic Peninsula, *J. geophys. Res.*, **95**, 6759–6777.
- Goldring, D.C., 1959. Falkland Island Dependencies Survey Preliminary Geological Report No. 2. The Geology of the Loubet Coast, Graham Land.
- Goldring, D.C., 1962. *The Geology of the Loubet Coast, Graham Land*, Vol. 36, pp. 50, British Antarctic Survey Scientific Reports no. 36.
- Golynsky, A. *et al.*, 2001. ADMAP—magnetic anomaly map of the Antarctic, 1:10 000 000 scale map, in *BAS (Misc) 10*, eds Morris, P. & von Frese, R., British Antarctic Survey.
- Griffiths, C.J. & Oglethorpe, R.D.J., 1998. The stratigraphy and geochronology of Adelaide Island, *Antarct. Sci.*, **10**, 462–475.
- Gunthner, W.R., Barbeau, D.L. Jr, Reiners, P.W. & Thomson, S.N., 2010. Slab window migration and terrane accretion preserved by low-temperature thermochronology of a magmatic arc, northern Antarctic Peninsula, *Geochem. Geophys. Geosyst.*, **11**, doi:10.1029/2009GC002765.
- Haselwimmer, C.E., Riley, T.R. & Liu, J.G., 2010. Assessing the potential of multispectral remote sensing for lithological mapping on the Antarctic Peninsula: case study from eastern Adelaide Island, Graham Land, *Antarct. Sci.*, **22**, 299–318.
- Hinze, W.J., Von Frese, R. & Saad, A.H., 2013. *Gravity and Magnetic Exploration, Principles, Practices and Applications*, Cambridge Univ. Press.
- Hole, M.J. & Larter, R.D., 1993. Trench-proximal volcanism following ridge crest-trench collision along the Antarctic Peninsula, *Tectonics*, **12**, 897–910.
- Hole, M.J., Rogers, G., Saunders, A.D. & Storey, M., 1991. Relation between alkalic volcanism and slab-window formation, *Geology*, **19**, 657–660.
- Jezek, K. & RAMP-Product-Team, 2002. RAMP AMM-1 SAR Image Mosaic of Antarctica. Fairbanks, AK: Alaska Satellite Facility, in association with the National Snow and Ice Data Center, Boulder, CO.
- Johnson, A., 1997. Cenozoic tectonic evolution of the Marguerite Bay area, Antarctic Peninsula, interpreted from geophysical data, *Antarct. Sci.*, **9**, 268–280.
- Johnson, A., 1999. Interpretation of new aeromagnetic anomaly data from the central Antarctic Peninsula, *J. geophys. Res.*, **104**, 5031–5046.
- Johnson, A. & Swain, C.J., 1995. Further evidence of fracture-zone induced tectonic segmentation of the Antarctic Peninsula from detailed aeromagnetic anomalies, *Geophys. Res. Lett.*, **22**, 1917–1920.
- Jordan, T.A., Ferraccioli, F., Vaughan, D.G., Holt, J.W., Corr, H., Blankenship, D.D. & Diehl, T.M., 2010. Aerogravity evidence for major crustal thinning under the Pine Island Glacier region (West Antarctica), *Geol. Soc. Am. Bull.*, **122**, 714–726.
- Kincaid, C. & Griffiths, R.W., 2003. Laboratory models of the thermal evolution of the mantle during rollback subduction, *Nature*, **425**, 58–62.
- Larter, R.D. & Barker, P.F., 1991. Effects of ridge crest-trench interaction on Antarctic-Phoenix spreading: forces on a young subducting plate, *J. geophys. Res.*, **96**, 19 583–19 607.
- Leat, P.T., Scarrow, J.H. & Millar, I.L., 1995. On the Antarctic Peninsula batholith, *Geol. Mag.*, **132**, 399–412.
- Leat, P.T., Riley, T.R., Wareham, C.D., Millar, I.L., Kelley, S. & Storey, B.C., 2002. Tectonic setting of primitive magmas in volcanic arcs: an example from the Antarctic Peninsula, *J. geol. Soc. Lond.*, **159**, 31–44.
- Leat, P.T., Flowerdew, M.J., Riley, T.R., Whitehouse, M.J., Scarrow, J.H. & Millar, I.L., 2009. Zircon U-Pb dating of Mesozoic volcanic and tectonic events in north-west Palmer Land and south-west Graham Land, Antarctica, *Antarct. Sci.*, **21**, 633–641.
- McCarron, J.J. & Larter, R.D., 1998. Late Cretaceous to early Tertiary subduction history of the Antarctic Peninsula, *J. geol. Soc. Lond.*, **155**, 255–268.
- McCarron, J.J. & Smellie, J.L., 1998. Tectonic implications of fore-arc magmatism and generation of high-magnesian andesites: Alexander Island, Antarctica, *J. geol. Soc. Lond.*, **155**, 269–280.
- Morgan, J.P., Ranero, C.R. & Vannucchi, P., 2008. Intra-arc extension in Central America: links between plate motions, tectonics, volcanism, and geochemistry, *Earth planet. Sci. Lett.*, **272**, 365–371.
- Noltimier, K.F., 1998. Geological Analysis of ERS-1 SAR Mosaic: implications for the Tectonic Segmentation of the Antarctic Peninsula, 102 pages Byrd Polar Research Center Report No. 16, Byrd Polar Research Center, The Ohio State University, Columbus, OH.
- Parada, M.A., Orsini, J.B. & Ardila, R., 1992. Transverse variations in the Gerlache Strait plutonic rocks: effects of the Aluk ridge-trench collision in the northern Antarctic Peninsula, in *Recent Progress in Antarctic Earth Science*, pp. 395–403, eds Yoshida, Y., Kaminuma, K. & Shiraishi, K., Terra Publ..
- Pilkington, M. & Thurston, B.J., 2001. Draping corrections for aeromagnetic data: line versus grid-based approaches, *Explor. Geophys.*, **32**, 95–101.
- Piomallo, C., Becker, T.W., Funiello, F. & Faccenna, C., 2006. Three-dimensional instantaneous mantle flow induced by subduction, *Geophys. Res. Lett.*, **33**, doi:10.1029/2005GL025390.
- Ponce, D.A., Hildenbrand, T.G. & Jachens, R.C., 2003. Gravity and magnetic expression of the San Leandro Gabbro with implications for the geometry and evolution of the Hayward Fault Zone, Northern California, *Bull. seism. Soc. Am.*, **93**, 1–13.
- Ponce, D.A., Simpson, R.W., Graymer, R.W. & Jachens, R.C., 2004. Gravity, magnetic, and high-precision relocated seismicity profiles suggest a connection between the Hayward and Calaveras Faults, northern California, *Geochem. Geophys. Geosyst.*, **5**, Q07004, doi:10.1029/2003GC000684.
- Rajagopalan, S. & Milligan, P., 1994. Image enhancement of aeromagnetic data using automatic gain control, *Explor. Geophys.*, **25**, 173–178.
- Riley, T.R. & Leat, P.T., 1999. Large volume silicic volcanism along the proto-Pacific margin of Gondwana: lithological and stratigraphical investigations from the Antarctic Peninsula, *Geol. Mag.*, **136**, 1–16.
- Riley, T.R., Flowerdew, M.J. & Whitehouse, M.J., 2012. Chrono- and lithostratigraphy of a Mesozoic–Tertiary fore- to intra-arc basin: Adelaide Island, Antarctic Peninsula, *Geol. Mag.*, **149**, 768–782.
- Saltus, R., Blakely, R.J., Haeussler, P.J. & Wells, R.E., 2005. Utility of aeromagnetic studies for mapping of potentially active faults in two forearc basins: Puget Sound, Washington, and Cook Inlet, Alaska, *Earth Planets Space*, **57**, 781–793.
- Schellart, W.P., Freeman, J., Stegman, D.R., Moresi, L. & May, D., 2007. Evolution and diversity of subduction zones controlled by slab width, *Nature*, **446**, 308–311.
- Smellie, J.L., Moyes, A.B., Marsh, P.D. & Thomson, J.W., 1985. Reports on Antarctic field work: Geology of Hugo Island, Sooty Rock, Betbeder Islands and parts of the Biscoe and outcast Islands, *Br. Antarctic Surv. Bull.*, **68**, 91.
- Smith, G.P., Wiens, D.A., Fischer, K.M., Dorman, L.M., Webb, S.C. & Hildenbrand, J.A., 2001. A complex pattern of mantle flow in the Lau Backarc, *Science*, **292**, 713–716.

- Storey, B.C. & Garrett, S.W., 1985. Crustal growth of the Antarctic Peninsula by accretion, magmatism and extension, *Geol. Mag.*, **122**, 5–14.
- Thompson, M.R.A., 1972. New discoveries of fossils in the Upper Jurassic volcanic group of Adelaide Island, *Br. Antarctic Surv. Bull.*, **30**, 95–101.
- Turner, S. & Hawkesworth, C., 1998. Using geochemistry to map mantle flow beneath the Lau Basin, *Geology*, **26**, 1019–1022.
- Vaughan, A.P.M. & Storey, B.C., 2000. The eastern Plamer Land shear zone: a new terrane accretion model for the Mesozoic development of the Antarctic Peninsula, *J. geol. Soc. Lond.*, **157**, 1243–1256.
- Vaughan, A.P.M., Wareham, C.D. & Millar, I.L., 1997. Granitoid pluton formation by spreading of continental crust: the Wiley Glacier complex, northwest Palmer Land, Antarctica, *Tectonophysics*, **283**, 35–60.
- Vaughan, A.P.M., Wareham, C.D., Johnson, A. & Kelley, S., 1998. A Lower Cretaceous, syn-extensional magmatic source for a linear belt of positive magnetic anomalies: the Pacific Margin Anomaly (PMA), western Palmer Land, Antarctica, *Earth planet. Sci. Lett.*, **158**, 143–155.
- Vaughan, A.P.M., Eagles, G. & Flowerdew, M.J., 2012a. Evidence for a two-phase Palmer Land Event from cross-cutting structural relationships and emplacement timing of the Lassiter Coast Intrusive Suite, Antarctic Peninsula: Implications for mid-Cretaceous Southern Ocean plate configuration, *Tectonics*, **31**, TC1010, doi:10.1029/2011TC003006.
- Vaughan, A.P.M., Leat, P.T., Dean, A.A. & Millar, I.L., 2012b. Crustal thickening along the West Antarctic Gondwana margin during mid-Cretaceous deformation of the Triassic intra-oceanic Dyer Arc, *Lithos*, **142–143**, 130–147.
- Wendt, A.S., Vaughan, A.P.M., Ferraccioli, F. & Grunow, A.M., 2013. Magnetic susceptibilities of rocks of the Antarctic Peninsula: implications for the redox state of the batholith and the extent of metamorphic zones, *Tectonophysics*, **585**, 48–67.
- Woodcock, N.H. & Fischer, M., 1986. Strike-slip duplexes, *J. Struct. Geol.*, **8**, 725–735.
- Yegorova, T. & Bakhmutov, V., 2013. Crustal structure of the Antarctic Peninsula sector of the Gondwana margin around Anvers Island from geophysical data, *Tectonophysics*, **585**, 77–89.
- Yegorova, T., Bakhmutov, V., Janik, T. & Grad, M., 2011. Joint geophysical and petrological models for the lithosphere structure of the Antarctic Peninsula continental margin, *Geophys. J. Int.*, **184**(1), 90–110.

## SUPPORTING INFORMATION

Additional Supporting Information may be found in the online version of this article:

**Table S1.** Zircon U-Pb ion-microprobe geochronology data for samples from Sillard and Rigsby Islands.

**Figure S1.** Concordia diagrams showing U-Pb zircon geochronology results. Error ellipses are plotted with  $2\sigma$  uncertainties. Panels on the right show representative cathodo-luminescence (CL) images of dated zircon grains where the red ellipse shows the location of ion-microprobe analyses, the red text indicates the analysis spot number and the white text gives the corresponding  $^{206}\text{Pb}/^{238}\text{U}$  age in millions of years, with  $2\sigma$  uncertainties (<http://gji.oxfordjournals.org/lookup/suppl/doi:10.1093/gji/ggu233/-/DC1>).

Please note: Oxford University Press is not responsible for the content or functionality of any supporting materials supplied by the authors. Any queries (other than missing material) should be directed to the corresponding author for the article.